RADAR DATA ACQUISITION AND PROCESSING SYSTEM FOR UAV POSITIONING APPLICATIONS

by

Ömer Oğuzhan Başpınar

B.S., Electrical and Electronics Engineering, Boğaziçi University, 2019

Submitted to the Institute for Graduate Studies in
Science and Engineering in partial fulfillment of
the requirements for the degree of
Master of Science

Graduate Program in Electrical and Electronics Engineering
Boğaziçi University

2022

ACKNOWLEDGEMENTS

I would like to thank my thesis advisor Assoc. Prof. Ahmet Öncü for giving me the opportunity to conduct research and providing invaluable guidance throughout this work. They have inspired me by their sincerity, motivation and discipline. They have advised me in determining the extent of my research topic and the methodology I have put to use. They have helped me with presenting my work as clearly as possible.

I also would like to thank Berk Omuz for supporting me with their knowledge about the radar theory, microwave circuits and radar signal processing. Their opinions about the results of earlier experiments allowed me to improve my work and reach this point.

I would like to acknowledge the contribution of Erol Kayataş in the design, montage and aviating of the drone. They have devoted their limited time off their work to make the airborne measurements possible.

I am grateful to my family for their unending support and patience and their great faith in me. I would not be able to complete my study without their support.

I would like to acknowledge the support of Scientific and Technological Research Council of Turkey with National M.Sc. Scholarship Program during my graduate study.

This work was partially supported by the Scientific and Technological Research Council of Turkey under project number 119E203 with the title “Radar supported data acquisition and mapping for flying robots”, and Boğaziçi University research fund under project number 19002 with the title “Heavy-Lift UAV Design and Prototyping for Radars and Sensitive Payloads” and under project number 22A2ADP1 with the title “Research Project for AI-supported UAVs”.

ABSTRACT

RADAR DATA ACQUISITION AND PROCESSING SYSTEM FOR UAV POSITIONING APPLICATIONS

Small drones have started to be utilized by researchers for applications such as object tracking, imaging and remote sensing as they become more available, inexpensive and capable with the advancements in sensor and UAV technologies. Drones can be equipped with sensors such as cameras and radars. Radars can be used onboard for navigation aid by detecting range and velocity, as well as for radar imaging applications. Although the latter is common, they can be useful in navigation since they are barely affected by weather conditions or smoke. FMCW radars are fitting devices for drones since they are relatively simple and can be lightweight. Therefore, following a broad FMCW radar survey, a custom drone system and a radar system are designed and implemented for UAV positioning applications. A postprocessing algorithm for detecting the altitude above ground level and ground reflection is developed, and a range compensation method is proposed to improve the performance of the algorithm.

Results of a field experiment showed that the radar system can be used for airborne positioning applications. Detected altitudes show similarity to the flight video. Reflections coming from the metal objects are distinguished from those coming from the ground. Range compensation method enabled detecting much lower altitudes, and magnitude of ground reflections obtained from different altitudes became similar. The system can be used in landing aid applications with a proper autopilot software and in SAR imaging with a position sensor more accurate than GPS.

ÖZET

İHA KONUMLANDIRMA UYGULAMALARI İÇİN RADAR VERİ TOPLAMA VE İŞLEME SİSTEMİ

Duyucu ve İHA teknolojilerindeki gelişmelerin küçük uçan robotları daha ucuz, erişilebilir ve kabiliyetli kılmasıyla bunlar araştırmacılar tarafından imgeleme, nesne takibi ve uzaktan algılama gibi uygulamalarda kullanılmaya başlamıştır. Uçan robotlar kamera ve radar gibi duyucularla donatılabilirler. Radarlar uçan robot üzerinde mesafe ve hız tespiti yaparak yöngüdüme yardımcı olabilirler ya da radar imgeleme uygulamalarında kullanılabilirler. Bunlardan ikincisi yaygın olsa da, radarlar hava koşullarından ve dumandan oldukça az etkilendiklerinden yöngüdümde kullanımları faydalı olabilir. FMSD radarlar nispeten basit yapıda olduklarından ve hafif olabildiklerinden uçan robotlar için elverişlidirler. Bu durum üzerine, geniş bir FMSD radar araştırmasından sonra, İHA konumlandırma uygulamaları için özel tasarım bir uçan robot sistemi ile bir radar sistemi tasarlanıp gerçeklenmiştir. Yer seviyesine göre yüksekliği ve yerden gelen yansımaları tespit etmek için algoritma geliştirilmiş ve bu algoritmanın performansını artıracak bir menzil telafi yöntemi ileri sürülmüştür.

Saha deneyi sonuçları radar sisteminin hava kökenli konumlandırma uygulamalarında kullanılabileceğini göstermiştir. Tespit edilen yükseklikler uçuşun görüntü kayıtları ile benzerlik göstermektedir. Metal nesnelerden gelen yansımalar yerden gelen yansımalardan ayırt edilebilmiştir. Menzil telafi yöntemi çok daha düşük yüksekliklerin tespitini mümkün kılmış ve farklı yüksekliklerde edinilen yerden gelen yansımaları benzer büyüklüklere ulaştırmıştır. Sistem, uygun bir otomatik pilot yazılımı ile iniş yardımı uygulamalarında ya da KKS (GPS) duyucusundan daha doğru bir konum duyucusu kullanılarak SAR görüntüleme uygulamalarında kullanılabilir.

TABLE OF CONTENTS

ACKNOWLEDGEMENTS iii
ABSTRACT iv
ÖZET v
LIST OF FIGURES viii
LIST OF TABLES x
LIST OF SYMBOLS xi
LIST OF ACRONYMS/ABBREVIATIONS xiii
1. INTRODUCTION 1
1.1. Application Areas of Modern Drones 1
1.2. Sensor Systems for Drones 2
1.3. Drone Applications using FMCW Radar 5
2. FMCW RADAR THEORY 7
2.1. FMCW Radar Theory and Basics 7
2.1.1. Theory of Operation 7
2.1.2. Maximum Radar Range 10
2.1.3. Range Resolution 11
2.2. Radar Survey 11
3. DRONE RADAR SYSTEM 17
3.1. FMCW Radar Sensor 17
3.1.1. FMCW Radar Hardware 17
3.1.2. FMCW Radar Signal Processing 19
3.2. Acquisition and Processing Platform 20
3.2.1. Postprocessing 22
3.3. Drone Prototype 25
3.4. Overall System 29
4. EXPERIMENTAL RESULTS AND DISCUSSION 31
4.1. Experiment Setup 31
4.2. Results and Discussion 34

5. CONCLUSION 41
REFERENCES 44

LIST OF FIGURES

Figure 2.1. Frequency vs. time plots of transmitted and received chirps and resultant IF signal in a FMCW radar. 8

Figure 2.2. Building blocks of a simple FMCW radar. 8

Figure 3.1. Block diagram of the radar system. 17

Figure 3.2. Simplified processing steps of the FMCW radar for each virtual antenna. 19

Figure 3.3. ROS architecture on the host computer. 21

Figure 3.4. Block diagram of the drone system. 26

Figure 3.5. The flight controller, GPS module, radio receiver and telemetry module used on the drone system. 27

Figure 3.6. Top view of the drone frame. 27

Figure 3.7. Horizontal and inclined rotor and propeller examples used in the drone system. 28

Figure 3.8. Batteries and an example ESC module used in the drone system. . 28

Figure 3.9. Radar sensor, host computer and radar battery mounted on the drone system. 29

Figure 3.10. Block diagram of the overall system. 30

Figure 4.1. The setup and the scene with a corner reflector used for configuring the radar. 31

Figure 4.2. Illustration of the flight mission planned for the experiment. . . . 32

Figure 4.3. FMCW drone system, a radar target and a snapshot of the experiment. 33

Figure 4.4. Range profile against time for the entire measurement and for the flight duration. 35

Figure 4.5. Detected altitude and reflection against time without range compensation. 35

Figure 4.6. Detected altitude and reflection against time without range compensation using a lower minimum altitude. 36

Figure 4.7. Range profiles when the radar observes an object, obtained with and without range compensation. 37

Figure 4.8. Range profile against time for the entire measurement with and without range compensation. 38

Figure 4.9. Detected altitude and reflection against time with range compensation. 38

Figure 4.10. Range profile against time for the flight duration with and without range compensation. 39

Figure 4.11. Detected altitude and reflection against time for the flight duration with range compensation. 40

LIST OF TABLES

Table 2.1. Properties of selected radar products for drone applications. 15

Table 4.1. Summary of useful radar parameters. 32

Table 4.2. Summary of the measurement flight. 34

LIST OF SYMBOLS

B	Bandwidth
c	Speed of light
f	Frequency
f_{out}	Frequency of the wave at mixer output
F_s	Sampling frequency
G	Antenna gain
i_{gnd}	Range bin index of the ground
i_{max}	Range bin index of maximum range of interest
i_{min}	Range bin index of minimum range of interest
k	Range compensation parameter
M	Number of observations used for calibration
N	Number of range bins
P_r	Received power
P_{rmin}	Minimum detectable power at receiver
P_t	Transmitted power
R	Radar range
R_{bin}	Range bin width
R_{gnd}	Altitude with respect to ground
R_i	Range value of a range bin
R_{max}	Maximum range
$R_{max}^{F_s}$	Maximum range limited by sampling rate
R_{max}^{SNR}	Maximum range limited by SNR
$R_{max}^{T_c}$	Maximum range limited by chirp period
R_{min}	Minimum range
R_{res}	Range resolution
S	Slope of frequency modulation
t	Time
t_d	Time delay between transmitted and received wave

T_c	Chirp period
x_{out}	Mixer output wave
x_{rcv}	Received wave
x_{tr}	Transmitted wave
γ_{gnd}	Ground threshold parameter
γ_{obj}	Object threshold parameter
Γ	Radar reflection level
Γ_{gnd}	Ground reflection
$\Gamma_{gnd,i}$	Ground reflection of an observation
Γ_i	Reflection of a range bin
$\Gamma_{i,comp}$	Compensated reflection of a range bin
$\Gamma_{th,gnd}$	Adaptive reflection threshold for ground
$\Gamma_{th,obj}$	Calibrated reflection threshold for object
λ	Wavelength
σ	Radar cross-section area

LIST OF ACRONYMS/ABBREVIATIONS

1D	One Dimensional
2D	Two Dimensional
3D	Three Dimensional
ADC	Analog to Digital Converter
API	Application Programming Interface
CFAR	Constant False Alarm Rate
CW	Continuous Wave
DC	Direct Current
DSP	Digital Signal Processor
DSS	DSP Subsystem
EIRP	Effective Isotropic Radiated Power
ESC	Electronic Speed Controller
FFT	Fast Fourier Transform
FMCW	Frequency Modulated Continuous Wave
FSK	Frequency Shift Keying
FSPL	Free-Space Path Loss
GNSS	Global Navigation Satellite System
GPIO	General-Purpose Input/Output
GPR	Ground Penetrating Radar
GPS	Global Positioning System
GUI	Graphical User Interface
HAGL	Height Above Ground Level
HDMI	High-Definition Multimedia Interface
HWA	Hardware Accelerator
IC	Integrated Circuit
IF	Intermediate Frequency
IMU	Inertial Measurement Unit
LED	Light-Emitting Diode

LNA	Low-Noise Amplifier
LPF	Low Pass Filter
LVDS	Low Voltage Differential Signaling
MCU	Microcontroller Unit
MSS	Master Subsystem
NDT	Non-destructive Testing
PA	Power Amplifier
PLL	Phase-Locked Loop
PoE	Power over Ethernet
PWM	Pulse Width Modulation
RCS	Radar Cross-Section
RF	Radio Frequency
ROS	Robot Operating System
RTK	Real-Time Kinematic Positioning
RX	Receiver
SAR	Synthetic Aperture Radar
SDR	Software Defined Radio
SNR	Signal-to-Noise Ratio
SSH	Secure Shell Protocol
STW	See-Through-Wall
TX	Transmitter
UART	Universal Asynchronous Receiver-Transmitter
UAV	Unmanned Aerial Vehicle
USB	Universal Serial Bus
UWB	Ultra-Wide Band

1. INTRODUCTION

Unmanned Aerial Vehicles (UAV), or commonly known as drones, are flying robots which are either piloted remotely or able to fly on varying degrees of autonomy in order to fulfill a wide variety of missions. They are used in tasks that endanger human lives or are mundane [1]. They have seen a rise in popularity during previous few decades as they have become cheaper than ever.

Although their usage in military applications remains since their existence, UAVs are now used in commercial and scientific applications as well as in everyday life [2]. They are used in the areas such as aerial photography & movie making, agriculture, archaeology, glaciology, infrastructure and building inspection, logistics, military assault & reconnaissance, mine detection, object tracking, remote sensing, search & rescue, surveying & mapping, urban traffic analysis [2–4].

1.1. Application Areas of Modern Drones

Early development of UAVs aimed military usage such as assault and reconnaissance missions as they eliminate the necessity of an onboard human pilot. They required heavy engines to be able to carry heavy payloads. As the size and weight of the equipment reduced with technological advancements, size and cost of the UAVs have shrunk over time, allowing their area of utilization to spread [2].

Modern UAVs come in a wide range of forms, sizes and capabilities. They are designed to meet the needs of their mission. Medium and large UAVs are designed to fly at altitudes as high as kilometers, can fly for tens of hours for ranges of hundreds of kilometers. To meet these specifications, they need to be big in size and weight, hence they are very costly. Small and very small UAVs, however, do not need to carry heavy payloads or to fly long ranges, which makes them lightweight and hence, cheaper.

Multicopters are types of drones with multiple rotary-wings which let them to have simpler controllers, which allows flexible design, and high maneuver capability than fixed-wing drones, and the ability of vertical takeoff and landing. They can travel to otherwise inaccessible areas. Combining these features with the low cost that comes with small size and their ease of use, they have become popular.

In addition to their commercial use-cases such as filmmaking and logistics, military applications such as surveillance [5], modern UAVs have started to be used in research. Some of the application areas of UAVs in research are search and rescue [6], forest monitoring [7], object tracking [1, 3], ground observation and mapping [4], urban traffic analysis [8], precision agriculture [9], remote sensing applications such as in glaciology [10] and archaeology [11], non-destructive testing (NDT) and buried object detection [12–18], civil infrastructure and building inspection [19], radar imaging [20–23], antenna measurements [24, 25]. Some of the utilization areas of UAVs are illustrated in [2] as well.

1.2. Sensor Systems for Drones

Drones are equipped with many sensors. Certain types of the sensors are common in most drone systems, especially the ones which provide information critical for navigation. Combining the information obtained from these sensors, altitude and geographic orientation and position of the vehicle can be determined. Typical examples for these sensors are as the following:

- GPS (Global Positioning System) sensors are used to detect the geographical position of the vehicle by evaluating signals received from multiple satellites.
- An IMU (Inertial Measurement Unit) uses gyroscopes, accelerometers and magnetometers to obtain linear velocity and attitude of the vehicle.
- Compass is another type of sensor that uses the magnetic field of the Earth to obtain the orientation of the vehicle.

- Barometric pressure sensor is used to extract altitude of the vehicle using atmospheric pressure.

In accordance with its task, a drone may be equipped with other types of sensors to collect information about its environment. Ultrasonic sensors, lidars, cameras, thermal cameras, hyperspectral cameras, radars are examples of such sensors.

Ultrasonic sensors emit and collect ultrasound waves to detect distance and motion of the objects. They are used in obstacle avoidance applications on many robots and vehicles [26].

Cameras collect the visible light reflected from the objects to obtain an image of the area. They are widely used on drones as they provide useful information for applications of mapping and surveillance, in addition to more direct applications such as aerial photography, and there are relatively cheap options. Images obtained by camera-based sensors also make it easier to explain the data collected by other sensors which may be harder to be interpreted on their own.

Cameras sensors provide images understandable easily by humans, but their operation depends on the scene to be illuminated. Without the existence of another light source, like Sun in daytime, they cannot provide useful information. Opaque obstacles would block the view of cameras. Moreover, transparent objects such as glass cannot be detected by cameras as the visible light passes through them.

Thermal cameras use infrared radiation instead of visible light which is used by traditional cameras. As objects with higher temperature emit more infrared radiation, thermal cameras are useful in detecting objects hotter than its surrounding, such as living beings, overheating parts and fires.

Hyperspectral and multispectral cameras use continuous and spaced bands of the spectrum, respectively, to create images. They are useful in detection of the type of

material as they are able to use information coming in form of electromagnetic radiation outside of the visible spectrum.

Hyperspectral and multispectral cameras give more detailed information about the objects' reflection properties than that given by ordinary cameras, but they are very complex systems and therefore they are very expensive. They are also prone to the disadvantages of traditional cameras.

Lidars use the time of flight of visible light to detect the range of the objects. They are highly directional as they use lasers, which have very narrow beam. Lidars give extremely highly accurate range information and resolution. However, they cannot work under challenging weather conditions like heavy rain and fog due the the light being refracted. Transparency of objects is also a preventive issue.

Radar is another type of sensor that can be used on a drone. They use radio waves to detect the distance of objects. Radars can be used as altimeters or in Synthetic Aperture Radar (SAR) imaging applications on UAVs.

Radars eliminate the shortcomings of using visible light by using radio waves. Most importantly, they can work under challenging weather conditions. They can see through some types of materials and detect transparent objects [27]. Since radars illuminate their scene, they do not require an external radiation source. They are not affected by daylight and can work at night as well as at dark areas.

There are different radar technologies with different use cases. Some examples can be as following:

- Pulse radars emit pulses with a short duration, and wait for a longer duration so that echoes from further objects can reach before another pulse is sent. The distance of the object can be determined by detecting the time difference between the sent and received pulses.

- Continuous wave (CW) radars radiate radio signals continuously at a constant frequency. Reception of a signal at the frequency of interest shows existence of an object. Since the objects in motion would cause a Doppler frequency shift in the received signals, radial velocity of the object can be measured. Distance to the object, however, cannot be determined by purely this method as the signal is transmitted continuously and without any change in time.
- Frequency modulated continuous wave (FMCW) radars modulate the frequency of radio waves in time, allowing measurement of distance of the objects. Velocity of the objects can also be determined by comparing successive pulses.

FMCW radars have become very common and available. Since they have relatively simpler circuits than other types of radars, they can be small in size and cheap. They can also provide images by synthetic aperture radar (SAR) method [28–33] and can be used in terrain mapping applications [20,21]. As they can provide both distance and velocity information, they are used as automotive radars [34]. They can be used in automotive applications such as blind-spot detection, lane change and park assistance, as well as secondary applications such as occupancy detection and driver vital sign monitoring [35]. Using the penetration capability, FMCW radars can be used in applications such as ground penetrating radar (GPR) [11, 16–18] and see-through-wall (STW) radar [36, 37]. There are a number of remote sensing applications which use FMCW radars in literature as well [27, 38, 39].

1.3. Drone Applications using FMCW Radar

FMCW radars are suitable to be used onboard small drones since they also can be small and lightweight. Moreover, they are also cheap as they do not require complicated circuits. They are able to extract distance and velocity information which may help the navigation of the drone, just as they do in automotive applications described before.

Lately, FMCW systems are started to be used onboard UAV systems. Exploiting the high-resolution imaging capabilities of FMCW radars on such mobile platforms en-

ables various monitoring applications. There are several studies where SAR technique is used with FMCW radars on drones, some of which only involves the design of a radar system as such while others are aimed at terrain mapping and imaging applications [20,21,30–33,40]. There are also studies that use FMCW drone systems for GPR applications [11,16], some of which uses SAR technique as well [17,18]. However, apart from a few commercial drone systems that use the radar for obstacle avoidance, there is no drone system that uses an FMCW radar system in positioning or navigation. This may stem from the fact that small drones that can carry a radar system with sufficient computational power are newly developing. The systems mentioned before mostly use FMCW radars to obtain radar data and transfer the measurements to a ground station for processing, instead of involving an onboard processing platform. In this work, a drone system equipped with radar is proposed to be used for positioning applications.

2. FMCW RADAR THEORY

Radar is an acronym for *"Radio Detection and Ranging"*. As the name suggests, radar systems are used to detect if there is any object in its field of view, and estimate the distance between the radar and the object, if it exists. Radars use radio waves, typically between 3MHz and 100GHz, for this purpose. Using the time of flight of the radio waves and the speed of propagation in that medium, mostly air, the distance between the target and the radar can be calculated.

Radar systems are designed to detect at least one of the properties among the existence, motion, distance, velocity, angular position of the targets of interest, depending on the technique they use. For example, CW radars cannot detect static objects as their operation relies on Doppler shifts caused by their relative velocity. They cannot detect distance to an object since they have no way of knowing the time of flight, whereas FMCW radars modulate the frequency with time, hence they are able to detect the range of an object by detecting time delay using the frequency difference between the transmitted and received waves.

2.1. FMCW Radar Theory and Basics

2.1.1. Theory of Operation

FMCW radars modulate the frequency of the signal over time as in Figure 2.1 to obtain a chirp signal which enables target detection at range. Conventional pulse radars determine the time delay of outgoing and incoming pulses to determine the target range.

The time delay between the transmitted and received wave can be calculated by

$$t_d = \frac{2R}{c}, \tag{2.1}$$

where R is the range, t_d is the time delay between transmitted wave and received radar echo and c is the speed of light. Detection of this time delay between the outgoing wave and the incoming wave requires advanced electronic equipment. The most important reason why FMCW radars have become popular in recent years is that this time delay makes it possible to detect with simpler circuits. Figure 2.2 shows basic building blocks of a typical FMCW radar implementation.

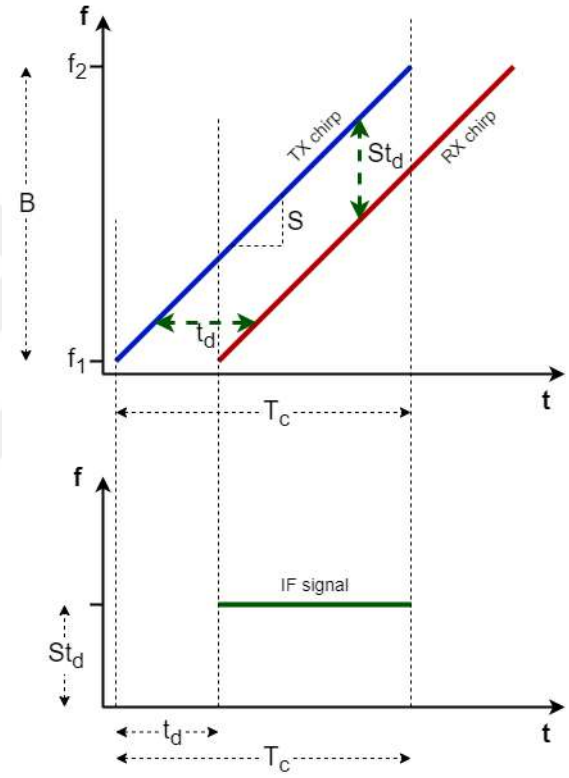

Figure 2.1. Frequency vs. time plots of transmitted and received chirps and resultant IF signal in a FMCW radar.

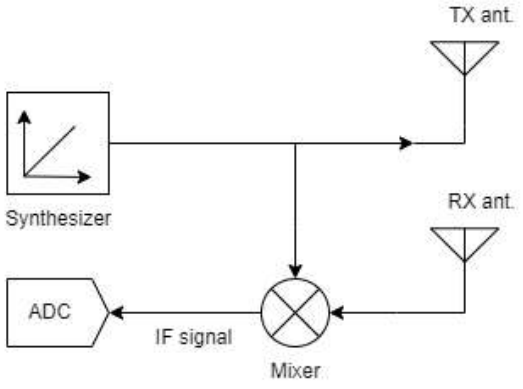

Figure 2.2. Building blocks of a simple FMCW radar.

In FMCW radar, the wave emitted by the transmitter can be defined as

$$x_{tr}(t) = cos(2\pi(f_1 + \frac{f_2 - f_1}{T_c}t)t), \tag{2.2}$$

whereas the received wave is

$$x_{rcv}(t) = cos(2\pi(f_1 + \frac{f_2 - f_1}{T_c}(t - t_d))t), \tag{2.3}$$

where f_2 represents the highest frequency of the chirp and f_1 represents the lowest frequency, T_c represents the pulse width or a period of the wave, and t_d represents the delay of the received wave. The bandwidth of the system B can be defined as $f_2 - f_1$. Mixing the outgoing and incoming waves and then applying a low pass filter (LPF) to eliminate high frequency components, the output will become

$$x_{out}(t) = cos(2\pi(\frac{f_2 - f_1}{T_c}t_d)t). \tag{2.4}$$

Thus, a single tone sinusoidal is obtained at the output of FMCW radar circuitry. The frequency of this signal is proportional to t_d which can be used to determine the range of the target. Using Equation (2.1) to replace t_d, x_{out} becomes

$$x_{out}(t) = cos(2\pi(\frac{2B}{cT_c}R)t). \tag{2.5}$$

The linear relationship between the frequency of the signal and the range is also obtained as

$$f_{out}(R) = \frac{2B}{cT_c}R, \tag{2.6}$$

where B/T_c term is an important parameter in FMCW radar systems, showing the frequency slope, hence it is mostly expressed as S. Finally, range of an object can be determined by solving Equation (2.6) for R, resulting in

$$R = \frac{cT_c}{2B}f_{out}. \tag{2.7}$$

2.1.2. Maximum Radar Range

There are different parameters that limit the radar range in theory and in practice. The theoretical limit of the system is equal to the maximum range that the wave can travel during one period of the FMCW signal, $R_{max}^{T_c}$, given by

$$R_{max}^{T_c} = \frac{cT_c}{2}. \tag{2.8}$$

While creating the FMCW equations, it is assumed that the outgoing and incoming waves are in the same period. Considering practical values of the pulse duration, corresponding maximum range value becomes very high, hence this range value is limited by other parameters. Therefore, the assumption made before is valid.

Another parameter that limits the maximum range is the sample rate of the receiver. The maximum value that the frequency of the IF signal can reach is B, bandwidth. According to the Nyquist-Shannon sampling theorem, sampling frequency, F_s, of the ADC(Analog-to-Digital Converter) has to be at least twice this value so that no information is lost. Although ADCs with very high sampling rates are expensive, the range value that corresponds to the frequency value equal to the bandwidth in FMCW radars which work at relatively high frequencies becomes so high that in practice, other limitations on the maximum range value takes affect. Still, sampling rate of the receiver sets an upper limit on the frequency of the IF signal whereby on the range value that can be detected, $R_{max}^{F_s}$, which can be shown as

$$R_{max}^{F_s} = \frac{cT_c}{2B}\frac{F_s}{2}. \tag{2.9}$$

The radar range equation is also an equation used to calculate the maximum range of the radar based on the frequency, the power of the transmitted wave, antenna gains and the minimum detectable power level. This maximum range, R_{max}^{SNR}, can be stated as

$$R_{max}^{SNR} = \sqrt[4]{\frac{P_t G^2 \lambda^2 \sigma}{P_{rmin}(4\pi)^3}} \tag{2.10}$$

where P_t is the transmitted power, G is the antenna gain, λ is the wavelength of the

signal, σ is the radar cross-section (RCS) value of the object and P_{rmin} is the minimum power value at the receiver that can be detected.

The actual maximum range value is set by the most effective of these upper limits. Hence, the final value can be obtained by

$$R_{max} = min(R_{max}^{T_c}, R_{max}^{F_s}, R_{max}^{SNR}). \tag{2.11}$$

2.1.3. Range Resolution

Range resolution is the minimum difference of distances to a FMCW radar of two objects for them to be distinguishable. Since the distance is related to the frequency in FMCW radars, this corresponds to a frequency value. According to the Fourier transform theory, for two frequency components that are distanced by Δf to be resolvable, they need to be observed for at least $1/\Delta f$. Substituting for Δf by Equation (2.6), the chirp duration T_c can be stated as

$$T_c = \frac{1}{\Delta f} = \frac{cT_c}{2B}\frac{1}{R_{res}}, \tag{2.12}$$

where R_{res} is the range resolution. Simplifying this equation, R_{res} is obtained as

$$R_{res} = \frac{c}{2B}. \tag{2.13}$$

This equation shows that range resolution depends only on the bandwidth in a FMCW radar. The frequency components of sampled IF signal can be calculated by using a Fast Fourier Transform (FFT) algorithm. Since the FFT output is in discrete form, resolution would be affected by the bin width of the transform. This can be surpassed by using FFT length of at least the number of samples per chirp.

2.2. Radar Survey

Small drones' strength comes from being inexpensive and easy to control. This, however, brings along some disadvantages. They cannot carry heavy or large payloads.

Large area of a payload can deteriorate aerodynamics of small drones. Heavy payloads require rotors to work at higher speeds, increasing power dissipation, thus shortening the flight duration.

A radar system needs to obey these limitations to be usable onboard a small drone. It needs to be small and lightweight. Furthermore, its power dissipation should be low as well since high power dissipation would necessitate the radar's battery to have large capacity, which means an increase in weight.

A literature survey is carried out in order to determine the approach to the radars used onboard UAVs. Researchers in [12–14, 22, 23] used UWB radar modules for UAV GPR, imaging and SAR applications, some of which were not available on market. In [21], an evaluation board of an automobile FMCW radar is used on a drone for terrain mapping with SAR techniques. A software defined radio (SDR) based radar is used in landmine detection in [15]. Researchers designed RF frontend for a FMCW radar and used a commercially available baseband board to test the antenna they have designed and manufactured for possible UAV applications in [40]. Custom-designed FMCW radars are used in [11, 16–18, 20, 29–33] for UAV GPR and SAR applications.

A comprehensive market survey about commercially available FMCW radars following the literature survey. Aim of this survey was to find radar systems which can be used in drone applications, with range detection capability, and can be used in radar signal processing applications. While all available products include RF frontend, they differ in specifications such as radar technology, detection capability, center frequency and bandwidth, output power, number of transmitter (TX) and receiver (RX) channels, data output and availability of raw data, requirement of additional circuits, prices. Some of these radar products can be summarized as below:

- IVS-362 is a radar sensor module which works between 24.00GHz and 24.25GHz frequency band using FMCW principles. It needs a control voltage input and outputs I-Q signals. This sensor involves 1 TX, 1 RX antenna with approximately

40° beamwidth. Output power is 15dBm. Additional circuitry to generate control voltage for frequency modulation and sampling is needed to use this sensor.

- K-LD7 is a Doppler radar sensor which works at 24GHz center frequency and 6dBm output power. It can detect distance of the moving objects using FSK (Frequency Shift Keying) technique, velocity and direction of moving objects using Doppler technique and angle of arrival as there are 2 RX antennas. Information about detected objects can be reached using serial data interface, as well as radar parameters can be changed. K-LD7-EVAL is the evaluation board of K-LD7 which allows raw data and FFT data to be stored and visualized via a GUI.
- K-MC4 is a Doppler radar with 18dBm output power at 24.00GHz - 24.25GHz frequency band. It has 1 TX, 2 RX antennas with 30°x12° beamwidth. This sensor produces analog output in I-Q form and allows FSK and FMCW techniques via its frequency modulation input. Sampling and control voltage generation circuitry are required.
- OPS243-C is a Doppler/FMCW radar with a start frequency of 24GHz and 20° beamwidth. It is capable of detecting range, velocity, motion and direction. Via UART-USB interface and a simple API, radar parameters can be changed and reports of detected objects can be collected. Raw and FFT data are available via API as well.
- Position2GO is the evaluation board of BGT24MTR12 FMCW transceiver IC, working around 24GHz start frequency. It can detect range, velocity, and angle of arrival of objects using 2 RX antennas with 76°x19° field of view. Operations such as PLL control and signal processing are done on its ARM Cortex-M4 based microcontroller. Communication is done using USB interface. Using a GUI which works on Windows, user can visualize the output of the radar and develop algorithms. Source code of the radar algorithms and firmware are available.
- IWR1843BOOST is an evaluation board of an industrial FMCW radar transceiver IC. The frequency band of this radar is between 76GHz and 81GHz with 4GHz continuous bandwidth and 12dBm output power. There are 3 TX, 4 RX antennas with 56°x28° beamwidth. This radar board has an integrated ARM R4F-based

MCU and an integrated DSP. It is capable of detecting range, velocity, angle of arrival information of detected objects. An API, firmware source code, examples and documentation are available. UART/USB can be used for communication, although there are many other interfaces. Raw data is streamed via LVDS interface, which can be converted to Gigabit Ethernet via an additional board.

- EV-RADAR-MMIC2 is a development board which involves transmitter, receiver and PLL ICs. RF frontend is designed to operate using FMCW technique at 24GHz start frequency with 250MHz bandwidth. Another circuit board is required to program the ICs. There are 2 TX, 4 RX channel connections on the board. To put the fine FMCW performance of the frontend to good use, a sampling circuit with matching quality and external antennas are required, therefore this option would be expensive.
- sR-1200e is a CW/FMCW radar which works at a frequency interval between 24.00GHz and 24.25GHz, with output power between 10dBm and 19dBm. It makes range, velocity and angle of arrival measurements possible. It has 1 TX, 2 RX antennas with a beamwidth of 65°x24°. Power over Ethernet (PoE) interface is used for transmission of power and data. A GUI tool which eases tasks such as configuring the radar, visualizing data and declaring user functions, as well as examples and expert support becomes available with additional charges, although using API is without these is also possible. Even without the GUI, this is an expensive radar compared to others.

Some of the radars found are removed from consideration since the effort of designing and testing additional circuit necessities were too high. Likewise, radars without antenna or analog output also require additional circuitry, therefore they are removed as well. Simple radar modules, like the ones without phase-locked loop (PLL), would not give good FMCW performance, therefore they are also removed from consideration. Radars which lack some capability compared to the ones with similar prices or the ones which are more expensive than those with similar specifications are eliminated. Remaining candidates are compared according to the Table 2.1. Finally, IWR1843BOOST is deemed the most appropriate for this work among more than 60 candidates from 12

companies, considering its ease of use and good documentation, detection capabilities and 3D field of view, high bandwidth, ergo good range resolution, and the fact that [21] uses a very similar radar of the same company.

Table 2.1. Properties of selected radar products for drone applications.

Properties	**OPS241-B**	**OPS243-C**	**Position2GO**
Radar Technology	FMCW	FMCW Doppler	FMCW
Start Frequency	24GHz	24GHz	24GHz
Max. Bandwith	1GHz	250MHz	250MHz
Output Power	11dBm	11dBm	11dBm
Antenna Gain	7dBi	11dBi	12dBi
Field of View	78° x 78°	20° x 24°	79° x 19°
TX Antennas	1	1	1
RX Antennas	1	1	2
PLL	-	+	+
Power Dissipation	1.6W	1.8W	2.1W
Dimensions (mm)	53 x 59 x 12	75 x 90 x 12	50 x 45 (60)
Weight (g)	11	15	150
Interface	UART, USB	UART, USB, RS232	UART, USB
Range Detection	+	+	+
Velocity Detection	-	+	+
Angle Detection	-	-	Azimuth
Configurability	+	+	+
Programmability	-	-	MCU
ROS Support	+	+	-
Available Data	Raw, FFT	Raw, FFT	Raw, FFT
Notes	API	API, Cloud and Android App via WiFi/Bluetooth	Windows GUI, source code

Table 2.1. Properties of selected radar products for drone applications. (cont.)

Properties	**IWR1843BOOST**	**sR-1200e**
Radar Technology	FMCW	FMCW Doppler
Start Frequency	77GHz	24GHz
Max. Bandwith	4GHz	2.5GHz
Output Power	12dBm	19dBm (EIRP)
Antenna Gain	10.5dBi	
Field of View	56° x 28°	65° x 24°
TX Antennas	3	1
RX Antennas	4	2
PLL	+	+
Power Dissipation	12.5W	4.5W
Dimensions (mm)	132 x 106	114 x 87 x 43
Weight (g)	30	280
Interface	LVDS, SPI, I2C, UART, USB	Ethernet (with PoE)
Range Detection	+	+
Velocity Detection	+	+
Angle Detection	Azimuth, Elevation	Azimuth
Configurability	+	+
Programmability	MCU + DSP	+
ROS Support	+	-
Available Data	Raw, FFT	Raw, FFT
Notes	documentation, source code, examples, application data over USB, raw data stream requires DCA1000EVM and Gigabit Ethernet	expert support and Windows GUI (costly)

3. DRONE RADAR SYSTEM

A drone radar system to be used in positioning applications is proposed in this work. Overall system is composed of two subsystems: a radar data acquisition and processing system, and a drone system. Radar data acquisition and processing system, or radar system in short, is made up of a FMCW radar sensor and a host computer, both of which are powered by a 4S Li-Po battery. A block diagram of the radar system is given in Figure 3.1. It is used to obtain and process radar information whereas drone system is used to carry the radar and the host computer in the field experiments.

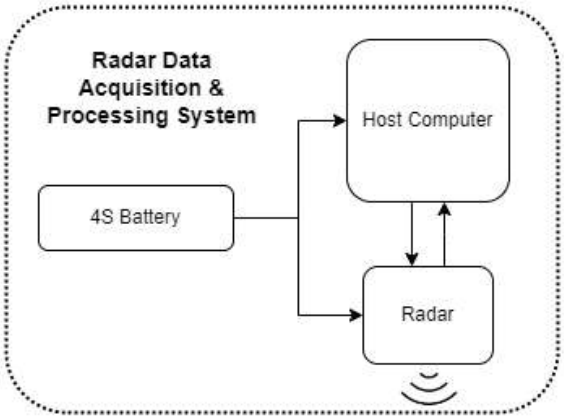

Figure 3.1. Block diagram of the radar system.

3.1. FMCW Radar Sensor

The radar sensor used in the design of the radar system is IWR1843BOOST. It forms the infrastructure of the radar system. It is a FMCW radar sensor that transmits and receives radar signals and outputs radar data in digital form.

3.1.1. FMCW Radar Hardware

At the core of the radar sensor board is IWR1843, a single-chip millimeter-wave industrial radar sensor with integrated MCU, DSP and radar hardware accelerator

(HWA). It operates in the 76GHz - 81GHz frequency band with up to 4GHz continuous chirp. It includes 3 transmitter (TX) and 4 receiver (RX) channels as well as built-in phase-locked loop (PLL) and analog-to-digital converters (ADC).

Radar IC can be divided into four subsystems: RF and analog subsystem, radio processor subsystem, master subsystem (MSS) and DSP subsystem (DSS). Functional block diagram of the radar IC can be seen in [41].

RF and analog subsystem consists of the RF and analog circuit parts, namely, the frequency synthesizer, power amplifier (PA), low-noise amplifier (LNA), mixer, intermediate-frequency (IF) filter and ADC, as well as crystal oscillator and some sensors. This subsystem can further be divided into transmit (TX) and receiver (RX) subsystems. The placement of the onboard antennas can be seen in [42]. Each 3 TX channels have a separate PA as well as phase-shifter for beamforming. Likewise, each 4 RX channels are identical, involving their separate LNA, mixer, IF filter and ADC circuits. As opposed to typical radar frontend implementations which use a real mixer with a real baseband and ADC chain, IWR1843 makes use of a quadrature mixer and complex-baseband architecture to provide complex I and Q outputs for each receiver channel. Using a complex-baseband architecture enables various advantages such as improved noise figure, improved interference tolerance, reduced impact of RF intermodulation products without any penalty in ADC interface rate or memory requirements [43].

Other subsystems consist of digital circuits. Radio processor subsystem involves digital filter chains, ADC buffer, chirp ramp generator and radio processor. MSS contains ARM Cortex-R4F-based processor and peripherals and it controls all device peripherals and house-keeping activities. Radar HWA helps calculations such as FFT and logarithms. DSS contains C674x DSP, a high-bandwidth interconnect, associated peripherals as well as L3 radar data memory. MSS and DSS can also be programmed by user.

3.1.2. FMCW Radar Signal Processing

FMCW radar theory is presented in Chapter 2. Equation (2.7) shows that the relationship between the range of an object and the frequency of IF signal is linear. This equation shows that range of the objects can be determined by detecting the peaks of FFT result. If there are multiple objects present at distances that differ by at least range resolution value, they appear as multiple peaks on the FFT. However, there might be multiple objects at the same distance which would fall into the same FFT bin. These objects cannot be distinguished by single observation. To overcome this issue, one can take multiple measurements which differ temporally or spatially. Since temporal diversities result from the changes in the range of the objects over time whereas spatial diversities arise from (concurrent) measurements taken at different positions, objects with similar ranges can be resolved by detecting radial velocities or angles of arrival.

The radar sensor is capable of detecting radial velocity by using a frame of successive chirps, called Doppler chirps, and angle of arrival by using multiple antennas. There are 3 TX and 4 RX channels on the radar. Each combination of TX and RX antennas forms a virtual antenna. For each Doppler chirp, each TX channel transmits the chirp signal one at a time and all RX channels receive reflected echo signals. Mixed IF signals are then sampled and saved into a section of the ADC buffer according to the virtual antenna of that observation.

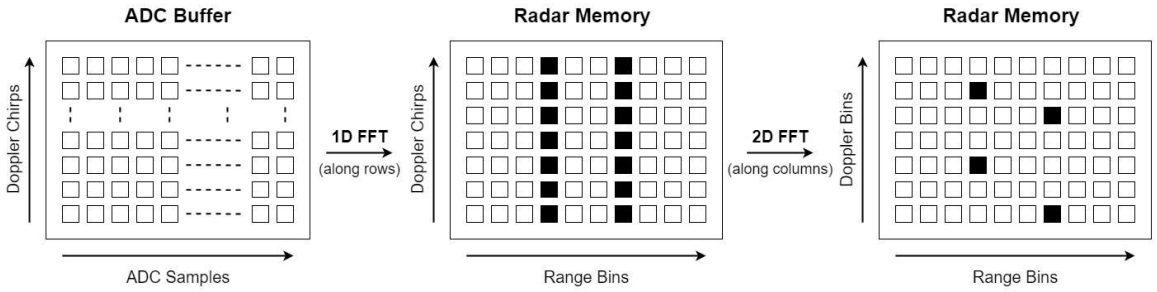

Figure 3.2. Simplified processing steps of the FMCW radar for each virtual antenna.

Figure 3.2 shows simplified steps of the radar signal processing for each virtual antenna. Samples obtained from each Doppler chirp are stored to the ADC buffer as rows. The first processing step is to compute FFT along the rows and save the output to the radar memory. This step is named 1D FFT and it is performed in parallel to the sampling process. As a result, data in the columns of the radar memory become range bins. Peaks along the rows indicate that high amount of reflections are collected from the corresponding range. Although the range bins at which the peaks occur are similar along the rows, the phase values at these peaks may not be the same and the difference is related to the radial velocity of an object.

After all the Doppler chirps are sampled into ADC buffer, processed by 1D FFT step and saved into radar memory, next step is performed: computing FFT along the columns of radar memory and storing the results into the radar memory. This step is called 2D FFT, or Doppler FFT, and the rows of the radar memory become Doppler bins. The rows will differ after this step. Peaks along the columns indicate that reflections coming from those distances are caused by objects with corresponding radial velocities.

The processing steps described above are performed on the data obtained by all virtual antennas. Theoretically, it is possible at this point to determine angle of arrival by performing a 3D FFT across virtual antennas. Then, log_2 of magnitudes for each virtual antenna are calculated and an accumulation is performed across virtual antennas. The result is a 2D matrix called *detection matrix*. The radar sensor transfers the range profile along the 0-Doppler bins via UART to the host computer.

3.2. Acquisition and Processing Platform

The other component of the radar system is the acquisition and processing platform, or host computer. NVIDIA Jetson AGX Xavier Development Kit is used as the host computer in the radar system. It is an embedded computer platform with 8-core ARM CPU, 512-core NVIDIA GPU and 64 Tensor cores, providing support

for computation-heavy applications. It comes with an Ubuntu-based (Bionic Beaver) operating system and it is supported by several SDKs and software libraries such as NVIDIA JetPack, CUDA, TensorRT. It is endowed with many ports such as Ethernet, USB, GPIO, HDMI, enabling connections to devices like radar and other types of sensors as well as to a monitor. It has a small form factor suitable for small drone applications and weighs around 500g including fan and heat sinks.

The software developed in this work uses ROS framework. Figure 3.3 shows the ROS architecture of the proposed system which runs on the host computer. In addition to *roscore*, there are two ROS nodes: *ti_radar_listener* and *ti_radar_recorder*. The former node is responsible from tasks such as

- extracting radar parameters from specified configuration file,
- checking the status of the radar,
- sending the configuration to the radar if it is not already configured,
- starting and stopping the radar,
- parsing incoming radar message frames,
- publishing incoming range profile data to ROS topic *ti_radar_rp*,
- publishing information about the detected objects to ROS topic *ti_radar_detobj*,

while the ladder node subscribes to ROS topics *ti_radar_rp* and *ti_radar_detobj* in order to store published messages into a measurement folder so that the information will be available for postprocessing.

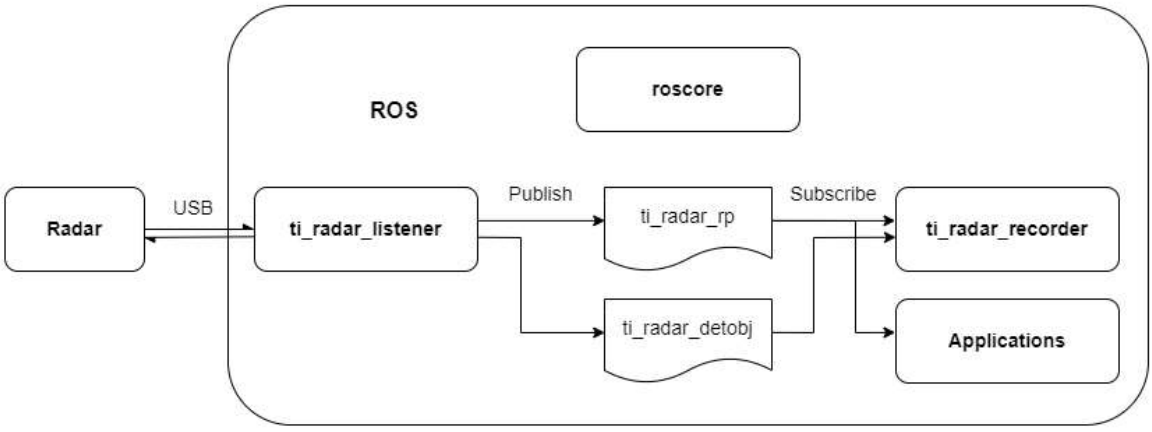

Figure 3.3. ROS architecture on the host computer.

3.2.1. Postprocessing

The range profiles generated by the radar sensor can be accessed by subscribing to *ti_radar_rp* topic in the ROS environment on the host computer. How these range profiles are processed in the first place by the radar sensor is described in Section 3.1.2. In this section, a postprocessing algorithm to detect the altitude and received radar reflection from that distance is presented. Here, the term *altitude* is used in the meaning of *height above ground level (HAGL)*. A processing step called *range compensation* is also proposed to overcome the difference in reflection values from varying distances.

Range profiles are formed by range bins, which are obtained by the FFT results of the FMCW radar output. The relation between the range value and the frequency is described before in Equation (2.7). Each range bin gives information about the level of reflections obtained from a range interval, hence the envelope of the range profile can be examined to detect the existence and the distance of an object, e.g. the ground or a metal object. A reflection threshold value for the ground $\Gamma_{th,gnd}$ can be determined by

$$\Gamma_{th,gnd} = \gamma_{gnd} + \frac{1}{N}\sum_{i=0}^{N-1}\Gamma_i \tag{3.1}$$

where Γ_i is the reflection value in dB at the ith range bin, N is the number of range bins in a radar frame, or FFT length, γ_{gnd} is an arbitrary ground threshold value that is determined according to the surroundings of the radar and kept constant for all radar frames in a measurement. The method used here is similar to the adaptive threshold of constant false alarm rate (CFAR) detection in that γ_{gnd} term in Equation (3.1) is chosen to keep the false alarm rate constant for an object whereas the second term on the right side of the equation forms the adaptive part of the threshold value.

The entire range profile may not be useful for a radar measurement. For example, the first few range bins inevitably contain near-DC terms of the IF signal. Effects such as antenna coupling can also be observed at short ranges. The reflection values at these near-DC may dominate the values at the remaining bins. Moreover, since

the furthermost range bins correspond to frequencies around the Nyquist rate, the information in these bins are less meaningful. Therefore, radar systems use a minimum and a maximum distance that useful information can be obtained. The marginal indices for the range bins of interest can be found as

$$\begin{aligned} i_{min} &= \lceil R_{min}/R_{bin} \rceil \\ i_{max} &= \lfloor R_{max}/R_{bin} \rfloor \end{aligned} \tag{3.2}$$

where R_{bin} is the range interval of a range bin, R_{min} and R_{max} are, respectively, arbitrary minimum and maximum range values of interest, i_{min} and i_{max} are nearest index numbers which correspond to R_{min} and R_{max}, respectively.

Examining the envelope of the range profile after the ground threshold and marginal indices are found, the index of the range bin that the ground reflections fall into, i_{gnd}, can be obtained by

$$i_{gnd} = min(i | \Gamma_i > \Gamma_{th,gnd}, i \in [i_{min}, i_{max}]). \tag{3.3}$$

Using this index, the altitude R_{gnd} can be found by

$$R_{gnd} = i_{gnd} R_{bin}, \tag{3.4}$$

and the ground reflection value Γ_{gnd} in the vicinity of the altitude can be chosen as

$$\Gamma_{gnd} = max(\Gamma_i | i \in [i_{gnd}, i_{gnd} + 4]). \tag{3.5}$$

The reasons for the small interval in Equation (3.5) are that in a digital Fourier transform (DFT), phasors are shared between successive range bins since the frequency values are discretized, and that the reflections from an object can fall into multiple range bins.

To detect the existence of an object that is more reflective than the ground, another threshold value for that object needs to be determined. For this, a calibration measurement can be done before the actual mission so that a mean value of the ground reflection from the desired altitude is obtained, and the reflection value obtained for

each observation in a measurement can be compared to the object threshold for object detection. The object threshold value $\Gamma_{th,obj}$ can be found by

$$\Gamma_{th,obj} = \gamma_{obj} + \frac{1}{M}\sum_{i=0}^{M-1}\Gamma_{gnd,i} \tag{3.6}$$

where $\Gamma_{gnd,i}$ is the ground reflection value obtained from the ith observation, M is the number of the observations used for calibration, γ_{obj} is an arbitrary object threshold value that depends on the reflective properties of the object, which can be determined by practical results.

The altitude and reflection detection methods described above use the range profiles as they are formed by the radar sensor. This methods are useful assuming the altitude of the drone is greater than a certain value and does not change too much. The reflections coming from an object may be lost within the clutter at low altitudes due to the aforementioned reasons that cause near-DC terms to be high. Another such reason is the free-space path loss (FSPL). It is the loss that is experienced by a signal as it propagates. The radar range equation takes this phenomena into account and so does the Equation (2.10) for calculating R_{max}^{SNR}. Received power P_r is proportional to $R^{1/4}$, according to the radar range equation. This means that signals are attenuated heavily with the distance. Signal amplitudes are high at short ranges, and amplitudes obtained from different ranges vary greatly, making comparisons difficult. Therefore, if the change in the drone altitude is relatively big during a flight, the reflection values would differ greatly. The FSPL may be compensated by some analog filters but the radar sensor used in this work does not perform such a filtering.

Each range bin is affected differently by a factor that affects the amplitude of the radar output signal depending on the frequency since the frequencies are transformed to ranges in a FMCW radar. One such factor is antenna gain. For example, the antenna gain of IWR1843BOOST is given as 10.85dB for 78.5GHz, and 9.59dB for 81GHz, i.e., there is approximately 1dB difference. Radar cross-section also depends on the frequency. Furthermore, the amount of reflections that reach the effective aperture

of the antenna also change with the distance to an object. Although their effect is slight except FSPL, each of these concepts influence the amplitude of the IF signal.

A processing step that may compensate for these affects would enhance the performance of the altitude and reflection detection methods. A method called *range compensation* is proposed to achieve this, which can be formulated as

$$\Gamma_{i,comp} = \Gamma_i + k \log_{10} R_i \tag{3.7}$$

where Γ_i and $\Gamma_{i,comp}$ are the reflection values at the ith range bin before and after the range compensation, respectively, R_i is the range value of the ith range bin, k is an arbitrary positive real number, the value of which can be determined practically. Since the reflection values are expressed in dB, Equation (3.7) actually multiplies each reflection value with a constant power of the corresponding range value. Note that after the calibration for determining the object threshold level, each observation can be processed separately with proposed methods, enabling navigation aid applications.

3.3. Drone Prototype

A drone solution is required to test the ability of the airborne radar system. Commercially available drones, although having good flight times and maneuver capabilities, are either expensive or cannot carry the payload formed by the proposed radar system. Moreover, one cannot access their flight control software, hence it is not possible to develop positioning applications using the data from the radar system. Therefore, a custom drone prototype is designed and built as a relatively inexpensive solution. A block diagram of the drone system is given in Figure 3.4.

At the core of the drone system is the Pixhawk Cube Orange autopilot, used as the flight controller. The autopilot hardware involves processors, sensors such as IMUs and barometers, and it provides interfaces for power supply and external sensor connections. It is responsible from the navigation of the drone, whether autonomous with a mission or controlled by a remote pilot. It evaluates sensory data from both

its internal sensors as well as external sensors, which are more reliable in most cases, such as GPS and barometer, then it generates control signals, PWM for this case, for electronic speed controllers (ESC). A stable version of the open source PX4 autopilot firmware is used on the flight controller.

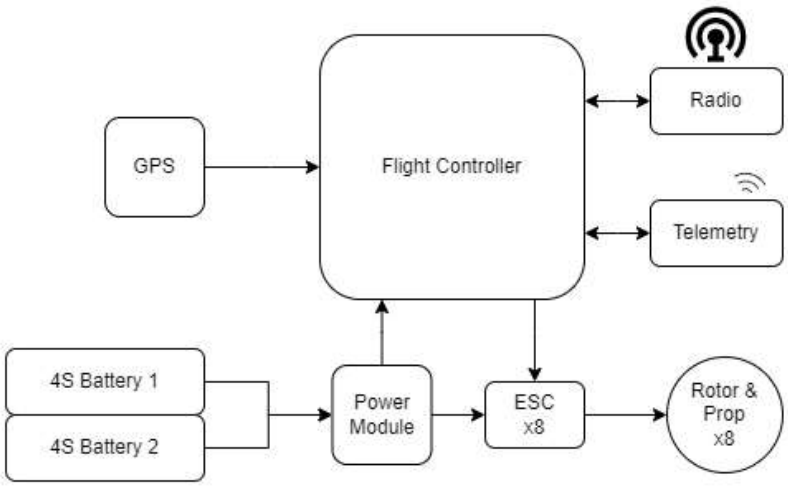

Figure 3.4. Block diagram of the drone system.

There are three types of receivers used in the drone system: a GPS, a telemetry module and a radio receiver. GPS module is the main positioning sensor used in this system, as it is the case for most drone systems. Pixhawk Here 2 GPS module is chosen since it is compatible with the autopilot. In addition to the GPS data, this module provides external sensor information such as compass and barometer, which greatly improves the positioning capability of the drone as the internal sensors of the flight controller are less accurate. A telemetry module is used to transfer flight missions that will be used in experimentation and to track the battery status and the position of the drone at the ground station. A radio receiver, RadioLink R9DS, is also used on the drone so that a remote pilot can take control of the drone in case of an emergency. Figure 3.5 shows the flight controller, GPS, radio receiver and telemetry modules used on the drone system.

Frame type of the drone is *OctoRotor X*, i.e., there are eight rotors placed symmetrically and equidistant from the center of the drone and the roll axis does not coincide with the rotors but rather with the midpoint of successive rotors. DJI 2312

960KV brushless DC motors are used in the design of the drone. The distance between each rotor and the center of the drone is 35cm. The diameter and height of the drone are around 1m and 50cm, respectively. There is a square area with edge lengths of 25cm at the middle of the drone, which is used to mount components of the drone system except ESCs and rotors. Front and rear sides of the drone are marked with red and blue, respectively, which can be seen in Figure 3.6.

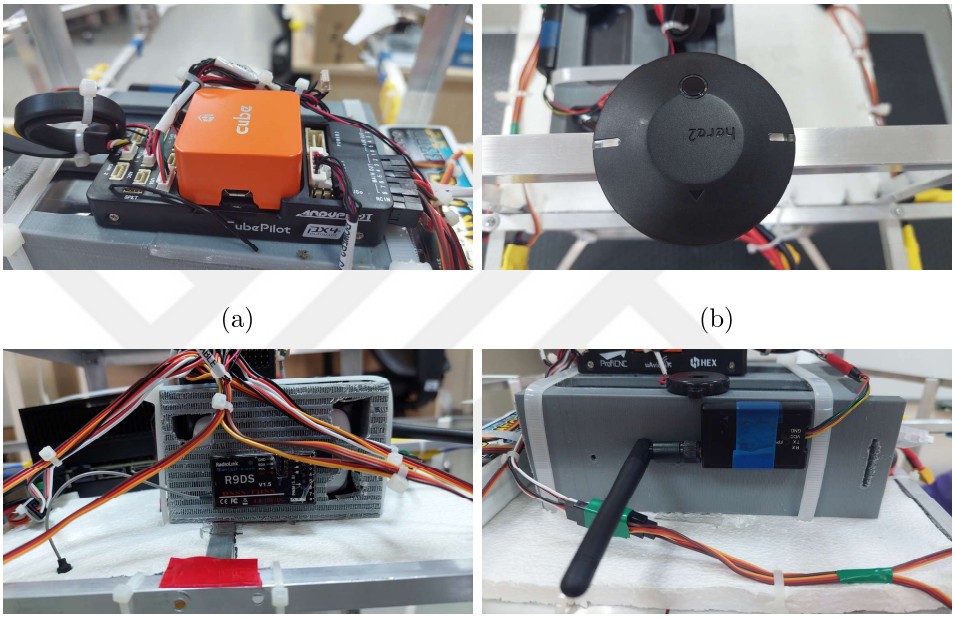

(a) (b)

(c) (d)

Figure 3.5. The flight controller (a), GPS module (b), radio receiver (c) and telemetry module (d) used on the drone system.

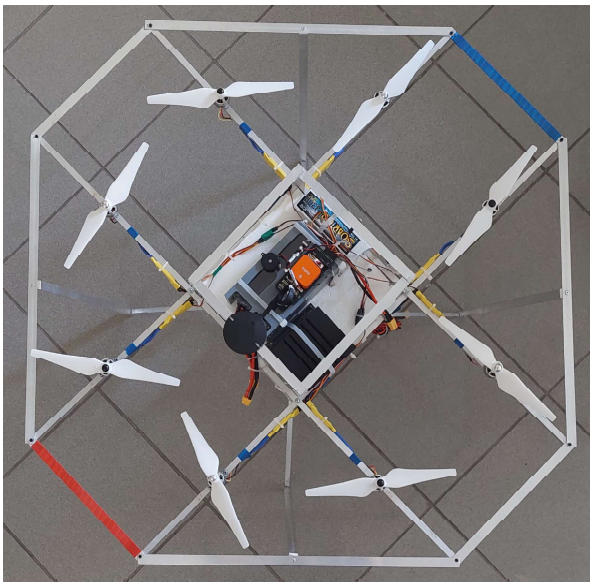

Figure 3.6. Top view of the drone frame.

In line with the earlier flight experiments, front and rear rotor pairs are inclined about 10° reciprocally in order to increase the resistance against light winds. Horizontal and inclined rotor and propeller examples are shown in Figure 3.7.

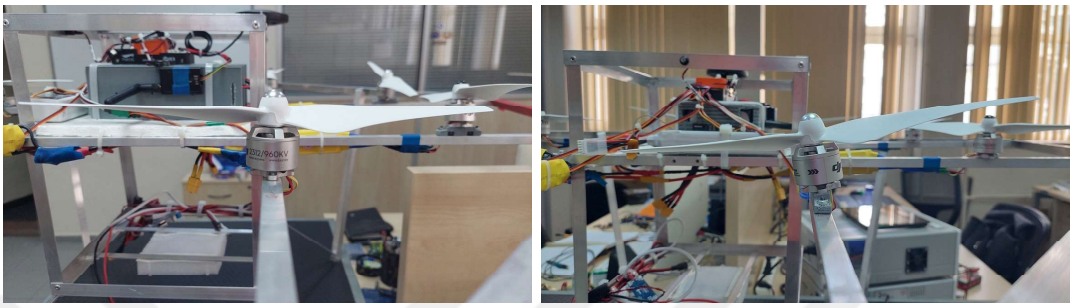

(a) (b)

Figure 3.7. Horizontal (a) and inclined (b) rotor and propeller examples used in the drone system.

To control eight independent rotors, as many electronic speed controllers (ESC) are required. An ESC converts the DC power coming from batteries to three-phase signal in accordance with the input signal from the autopilot. ESCs are placed between each rotor and the middle square, which can be seen in Figure 3.6. Also, an ESC example and the batteries in casing and is given in Figure 3.8.

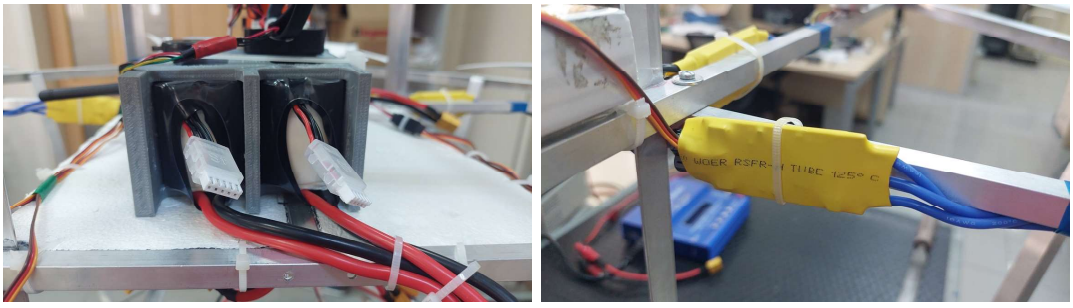

(a) (b)

Figure 3.8. Batteries (a) and an example ESC module (b) used in the drone system.

To supply electrical power to the rotors and the electronic components of the drone system, two 4S 5200mAh Li-Po batteries are used in parallel. Although a higher total battery capacity would provide more energy, the weight of the system increases with each battery as well. Therefore, one can find a sweet spot for the total battery capacity with the parts at hand that provides the best flight time. For this system, it

is found to be two identical 5200mAh batteries. A power module is used to sense the voltage and current coming out of the batteries and transfer this information together with a stepped-down voltage rail to the flight controller.

3.4. Overall System

Radar system needs to be mounted on the drone system for experimentation. Placement of the host computer and the battery of the radar system is important because these components are relatively heavy, hence they would affect the center of gravity of the overall system. Therefore, they are placed on the opposite sides of the diagonal on the middle square of the drone system. The radar sensor is mounted beneath the drone looking downwards. The distance from the radar to the bottom of the drone is 14cm. Figure 3.9 shows the components mounted on the drone system. Weight of the overall system is measured as 4.7kg.

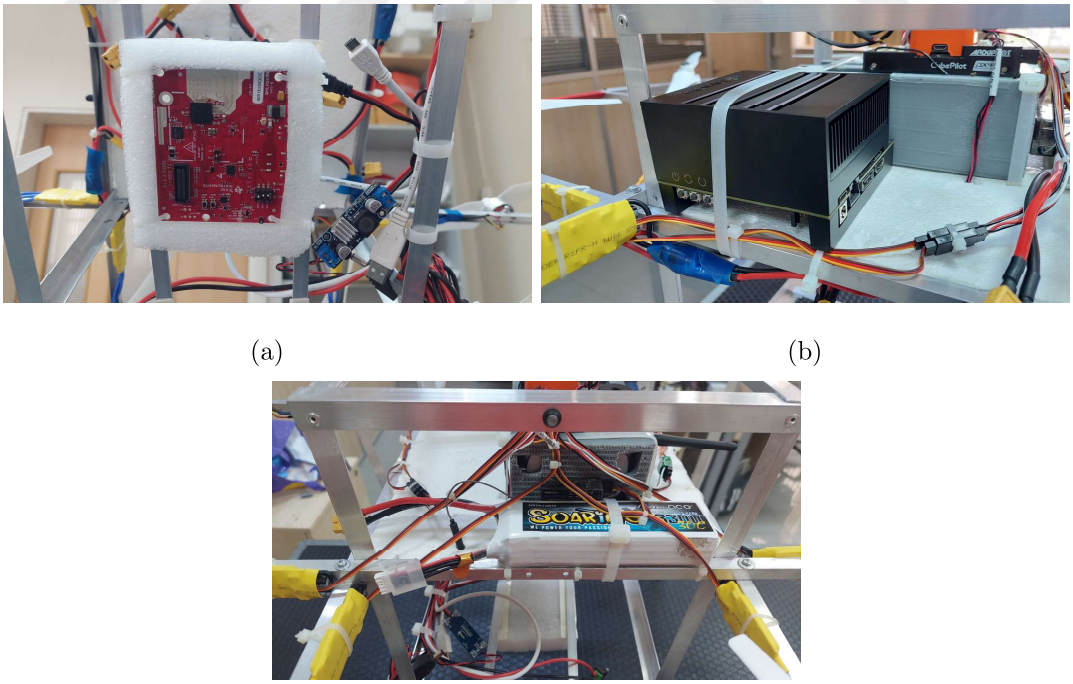

(a) (b)

(c)

Figure 3.9. Radar sensor (a), host computer (b) and radar battery (c) mounted on the drone system.

Overall system diagram is shown in Figure 3.10. A laptop with a telemetry module is used as the ground station and a remote (radio) controller is also present for emergencies. Before any measurement, an ethernet connection is established between the host computer and the ground station. A script file is executed on the host computer using SSH (Secure Shell Protocol) so that the measurement starts. The connection is then removed and a mission plan is uploaded to the autopilot. At this point, the mission can be started by the radio controller or the ground station.

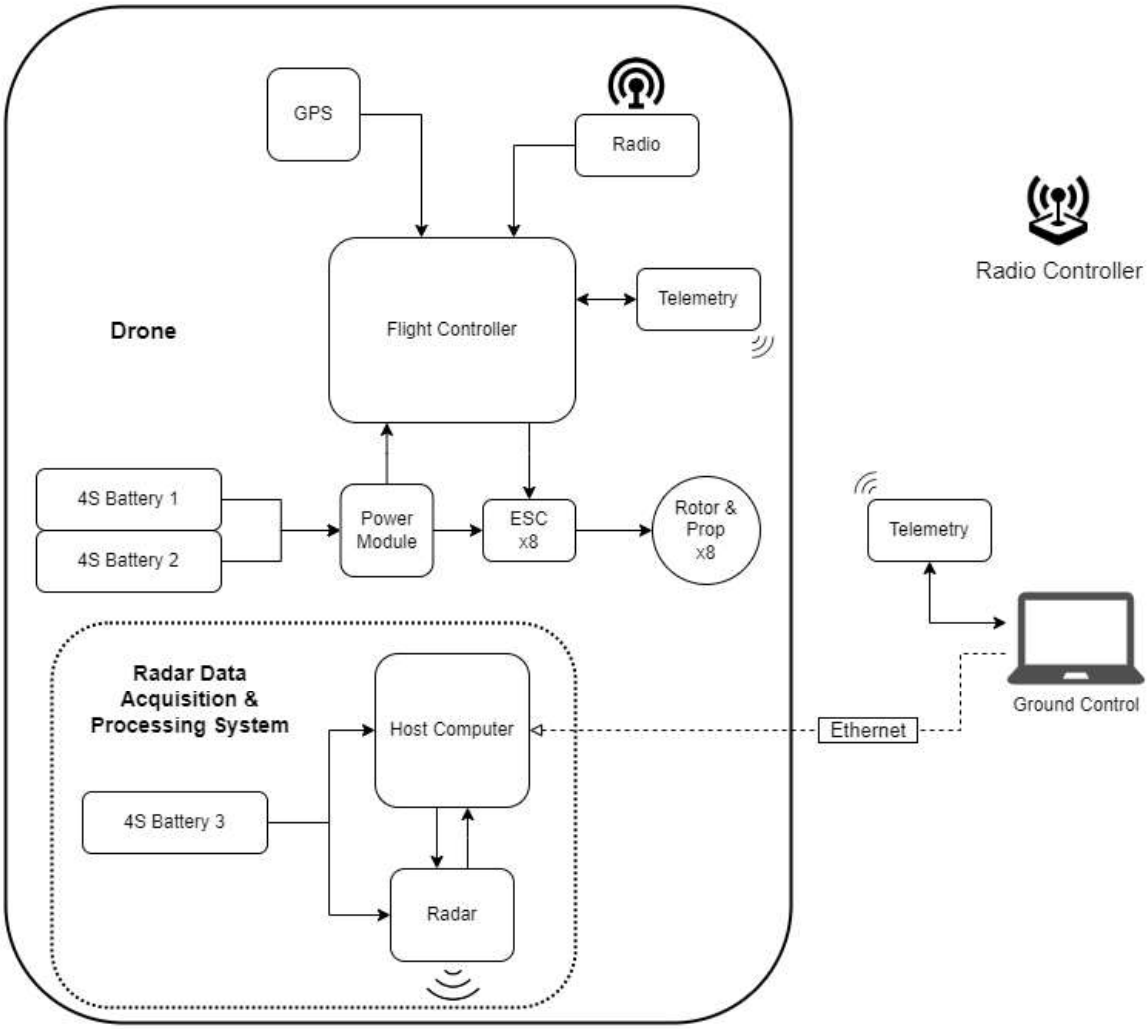

Figure 3.10. Block diagram of the overall system.

4. EXPERIMENTAL RESULTS AND DISCUSSION

Experimentation is required to show the functionality of both radar and drone subsystems. Radar system needs to be able to report the altitude, the existence of a reflective object and level of reflections obtained. Also, drone system should be able to carry the radar system for an airborne experimentation. Therefore, a field experiment is conducted on July 22, 2022 at the Uçaksavar Stadium of the Boğaziçi University.

4.1. Experiment Setup

The radar parameters need to be determined according to the needs of the experiment. To create a radar configuration file, a corner reflector, which is used as a radar target in the experiment, is put on the ground at 7m distance from the radar. The setup and the scene used for configuring the radar can be seen in Figure 4.1. Some of the useful configuration parameters are listed in Table 4.1.



(a) (b)

Figure 4.1. The setup (a) and the scene with a corner reflector (b) used for configuring the radar.

A flight route is created for the experiment using a ground control software, QGroundControl. Figure 4.2 illustrates the mission plan. Each circle indicates a waypoint whereas diamonds indicate waypoints with a radar target placed below. The drone is planned to hold its position for 10s at when it arrives the waypoints with dark grey markers, and 5s at those with light grey markers. The wait times are set to ease time-stamping the experiment using a video record as well as interpreting radar

measurements. The uncolored waypoint markers indicate that the drone will not stop but pass through those points. Also, the waypoints named *T, L, D* indicate *takeoff, landing, dummy* points, respectively. Dummy point is added to ensure the orientation of the drone before the actual mission starts. The height of the waypoints are chosen as 7m considering the radar configuration as well as the accuracy of GPS and barometer sensors.

Table 4.1. Summary of useful radar parameters.

Radar Parameter	**Value**
Frame Period	100ms
Range Resolution	0.044m
Max. Unambiguous Range	14.68m
Velocity Resolution	0.62m/s
Max. Radial Velocity	4.94m/s
FFT Length	512
FFT Bin Width	0.036m
RF Channels	3 TX / 4 RX

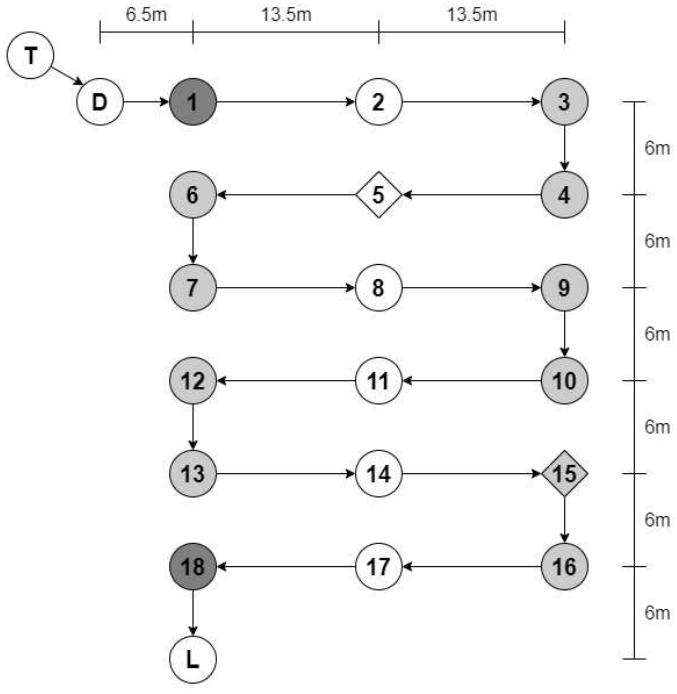

Figure 4.2. Illustration of the flight mission planned for the experiment.

The experiment is started after the configuration file is created and the flight mission is uploaded to the UAV. Radar system is started to take measurements and store the range profiles. Complete FMCW drone system and one of the two corner reflectors that are used as radar targets in the experiment are shown in Figure 4.3, together with a snapshot of the experiment while the airborne radar system is flying towards an object.

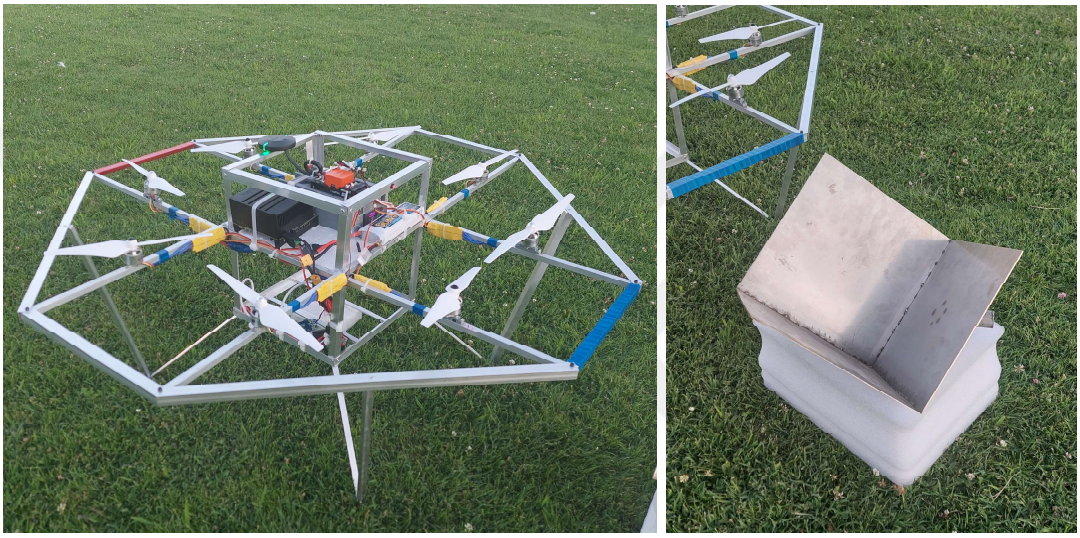

(a) (b)

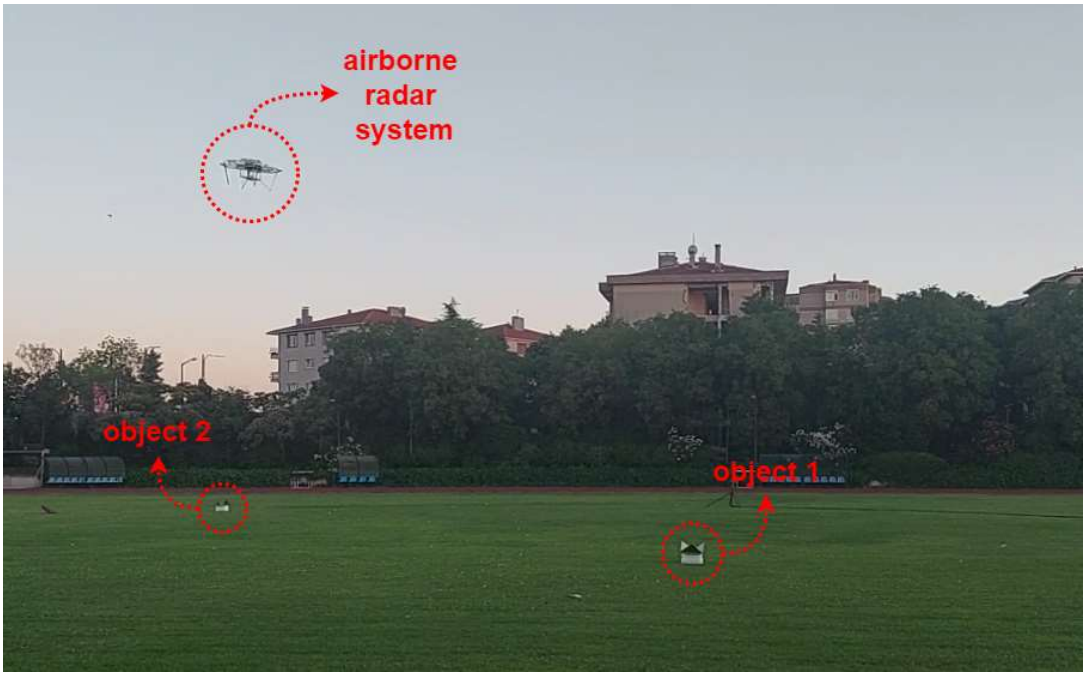

(c)

Figure 4.3. FMCW drone system (a), a radar target (b) and a snapshot of the experiment (c).

A video recording is taken during the flight. The drone is landed around waypoint 17 with a battery failsafe warning before the mission is completed. This is not an issue since both of the radar targets are flown over, hence the essential parts of the experiment were already completed at that point. A flight summary is given in Table 4.2.

Table 4.2. Summary of the measurement flight.

Parameter	**Value**
System Weight	4.7kg
Flight Altitude	$\sim$ 5.7m - 7.2m
Waypoints Arrived	17
Total Distance	$\sim$ 178m
Horizontal Velocity	$\sim$ 2.2m/s
Travel Duration	82s
Pos. Hold Duration	80s
Total Mission Duration	162s
Out of Mission Duration	10s
Takeoff Duration	6s
Landing Duration	13s
Flight Duration	191s

4.2. Results and Discussion

Range profiles recorded throughout the experiment are plotted against time without postprocessing in Figure 4.4(a). There are two distinct time periods which are meaningful: around $0s - 80s$ and around $140s - 360s$. The former is the time period that the drone is carried manually to the takeoff point in the measurement site. Then, it is put on the ground until the mission is started. The latter time period corresponds to the flight, which is shown in Figure 4.4(b).

The altitude of the drone during the flight can be tracked on Figure 4.4(b). The reflections coming from the radar target around waypoint 15, which is marked as

object 2 in Figure 4.3(c), can be seen between $297s - 308s$ around $6m - 7m$, and their harmonic signals around $12m - 14m$. The altitude change within this interval is also clearly captured in the video recording. The radar target around waypoint 5, which is marked as *object 1* in Figure 4.3(c), cannot be seen here clearly as it is swiftly flown over. However, it will be detected later.

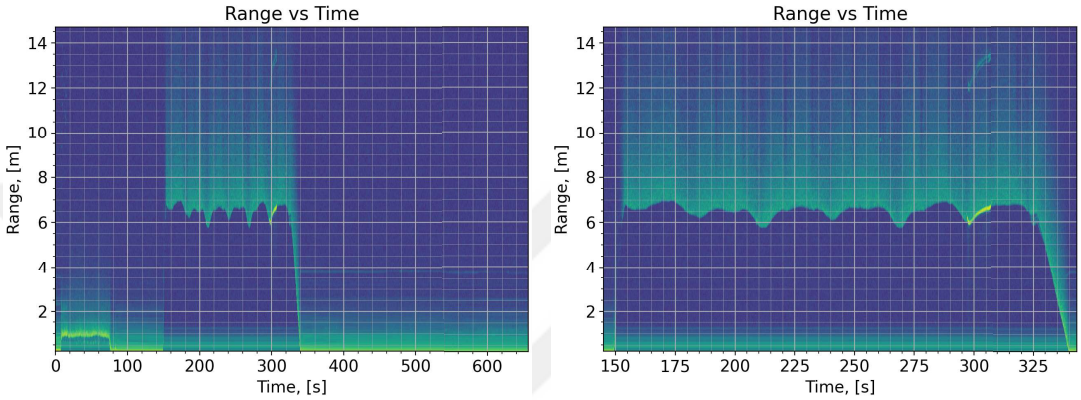

(a) (b)

Figure 4.4. Range profile against time for the entire measurement (a) and for the flight duration (b).

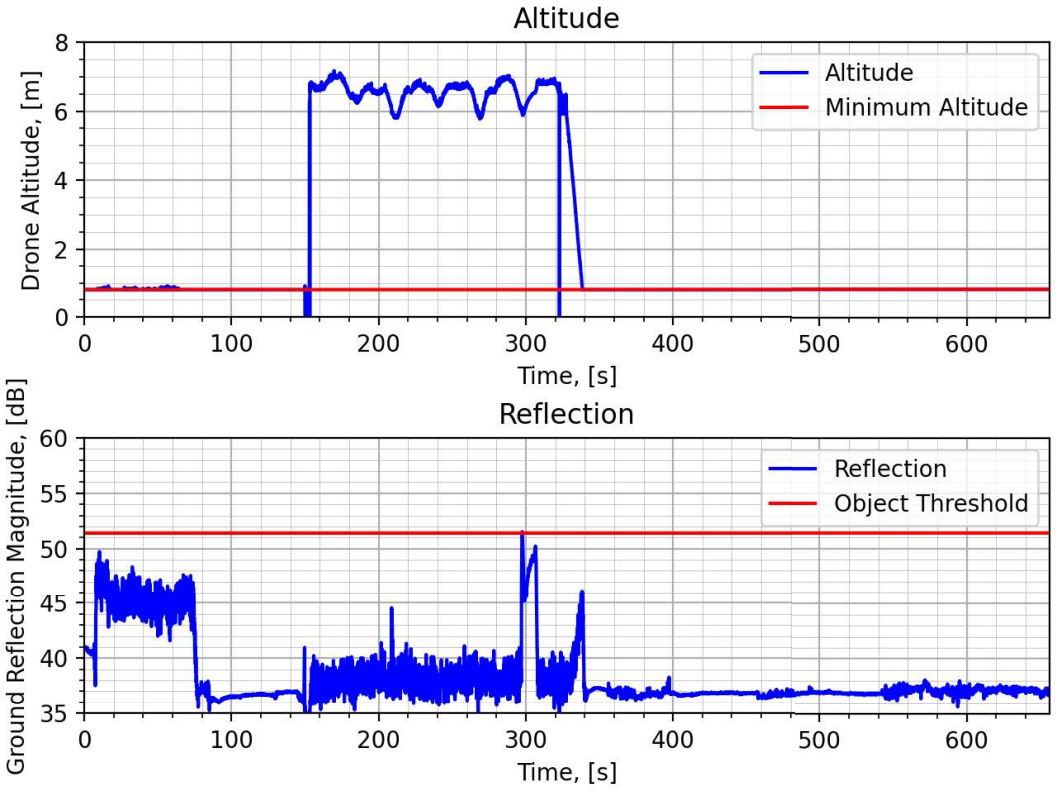

Figure 4.5. Detected altitude and reflection against time without range compensation.

The altitude and reflection detection methods described in Section 3.2.1 are applied to the range profiles. The results are shown in Figure 4.5. The minimum altitude value used in the postprocessing of this figure is 0.80m. The flight period of the altitude against time plot resembles the altitude that can be tracked on Figure 4.4(a), except at a few points around 320s where the altitude could not be detected, hence the plot goes to 0. Another such case is seen during the takeoff around 150s where the altitude detection starts, then it is disrupted and goes to 0, and continues afterwards. The reflection values detected during the flight are mostly around the same level as they are coming from ground level. Reflections from *object 2* are clearly visible. Also, there is a spike around 210s, which indicates the reflections coming from *object 1* as the drone was between waypoint 4 and waypoint 6 at that time according the video recording. The altitude and reflection values are also detected for the period in which drone is carried.

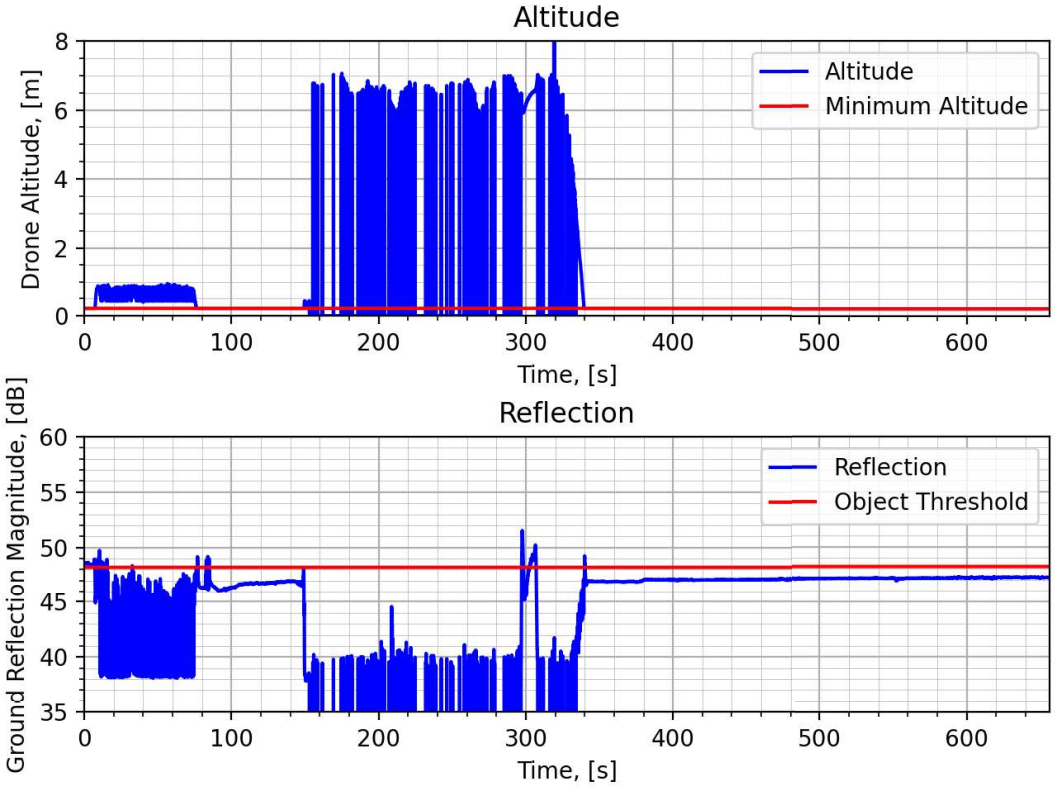

Figure 4.6. Detected altitude and reflection against time without range compensation using a lower minimum altitude.

The reflection magnitudes at ranges below $1m$ are seemed to be high in Figure 4.4. When minimum altitude value for detection is set to lower values, the altitude detection deteriorates since the near-DC terms start to become dominant as it is described in Section 3.2.1. Figure 4.6 shows such a case where the minimum altitude is set to be 0.20m. Moreover, the magnitudes of ground reflections obtained from approximate altitudes of $1m$ and $7m$ differ by around 7dB according to the Figure 4.5.

The range compensation method described in Equation (3.7) is applied to the range profiles in order to overcome the issues described above. Figure 4.7 shows the range profile obtained at $300.0s$, both before and after range compensation. A ground threshold level is also marked for both cases. It is clear that the minimum altitude value used in detection steps enhances with range compensation as the range bins at very low altitudes are suppressed. It is worth noting that the value of k in Equation (3.7) that gave the best results among several values is found to be 10, and an extensive grid search was not necessary since the obtained results are good enough.

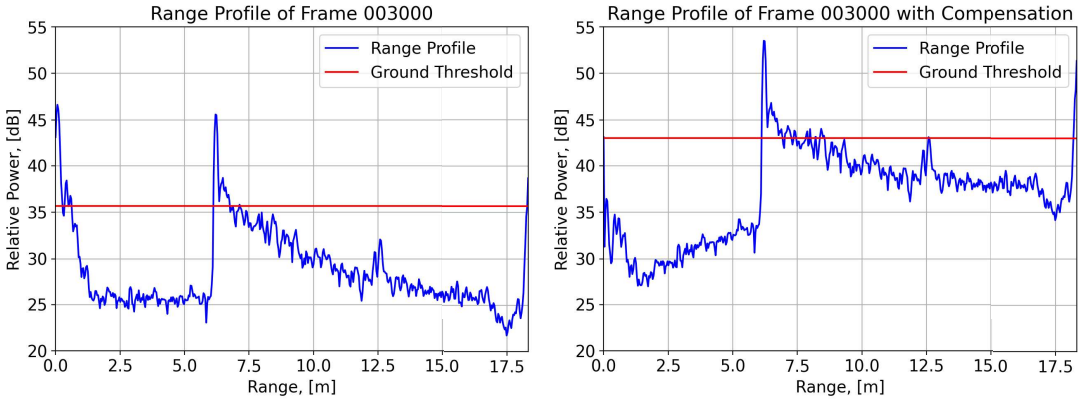

(a) (b)

Figure 4.7. Range profiles when the radar observes an object, obtained without (a) and with (b) range compensation.

Figure 4.8 shows the range profiles for the entire measurement, before and after range compensation. The plot becomes much clearer at short ranges after range compensation than it was before. Figure 4.9 shows the detected altitude and reflections after range compensation. The minimum altitude value is set to 0.20m.

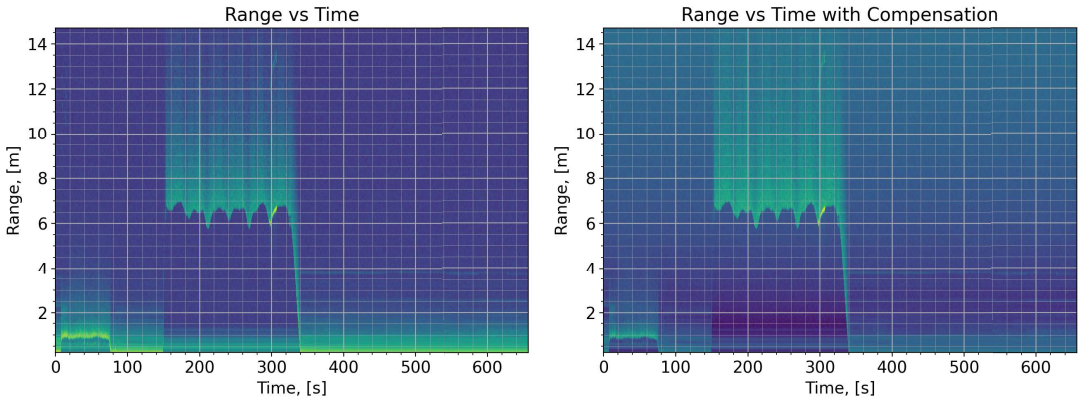

(a) (b)

Figure 4.8. Range profile against time for the entire measurement without (a) and with (b) range compensation.

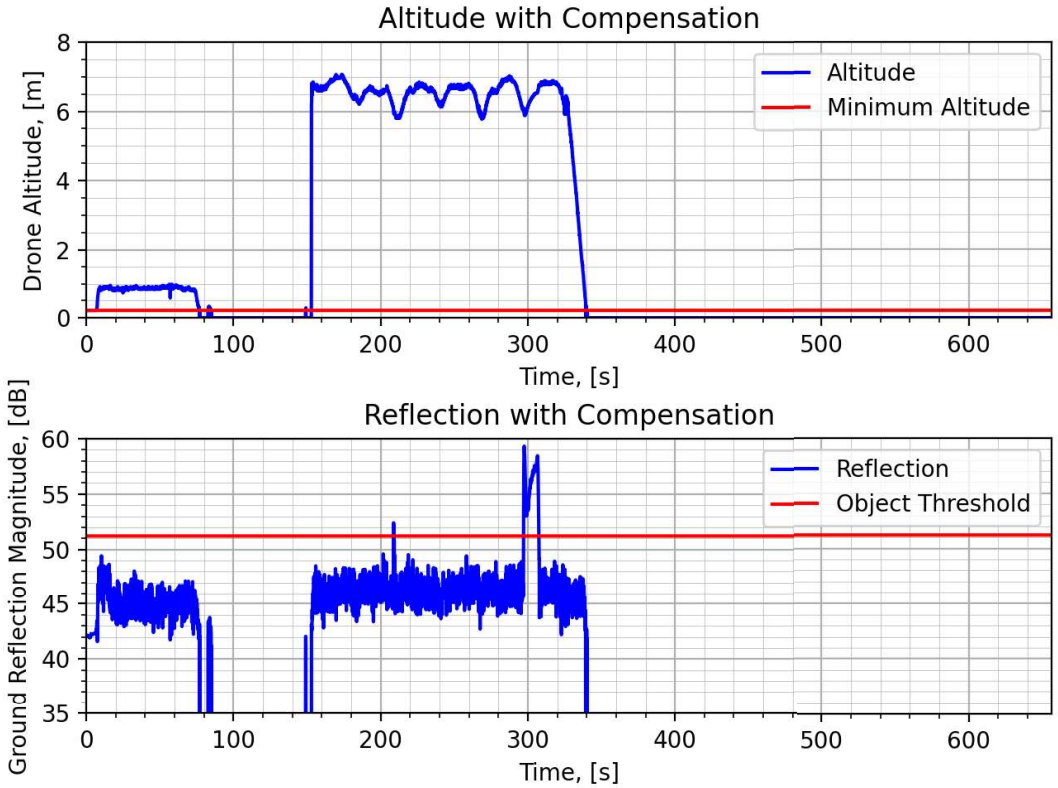

Figure 4.9. Detected altitude and reflection against time with range compensation.

The results in Figure 4.9 are way better than those in Figure 4.6, which uses the same minimum altitude value without performing range compensation. The altitude plot is similar to that in Figure 4.5, except the disruption around 320s no longer exists. The landing altitudes are almost completely observed as the distance between the radar and the bottom of the drone is 0.14m. Lifting and lowering of the drone during its

transport before the mission are started to be observed. Even the tilting of the drone to check the LEDs of the radar after it is put down is seen as a small spike around 80s. Magnitude levels of ground reflection became similar throughout the experiment. Furthermore, the threshold level for the objects became more apparent.

Finally, the range profiles for the flight period before and after range compensation are shown in Figure 4.10, and altitude and reflection values obtained for the same period after range compensation are demonstrated in Figure 4.11. One final remark is that the altitudes of the landing period are observed better than those of takeoff period. This results from the fact that the radar is programmed to transfer range profiles in the 0-Doppler bins. The altitude change in both periods are around 6.5m while the takeoff and landing durations are 6s and 13s, respectively, according to Table 4.2. The radial velocity of the ground during the takeoff and landing becomes 0.50m/s and 1.08m/s, respectively. Since the velocity resolution is 0.62m/s, which is given in Table 4.1, the ground reflections during the former period falls into the 0-Doppler bin while the latter does not. This can also be seen in Figure 4.10 where the track of ground reflections become almost indistinguishable in both cases during takeoff.

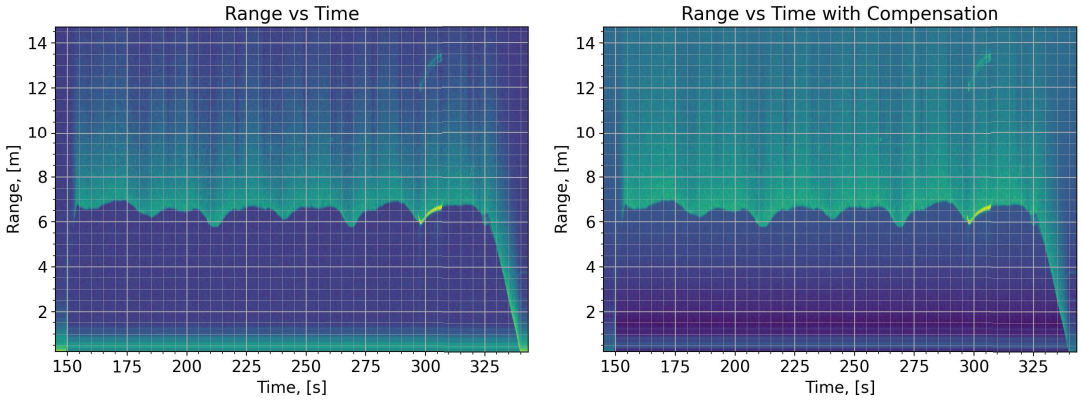

(a) (b)

Figure 4.10. Range profile against time for the flight duration without (a) and with (b) range compensation.

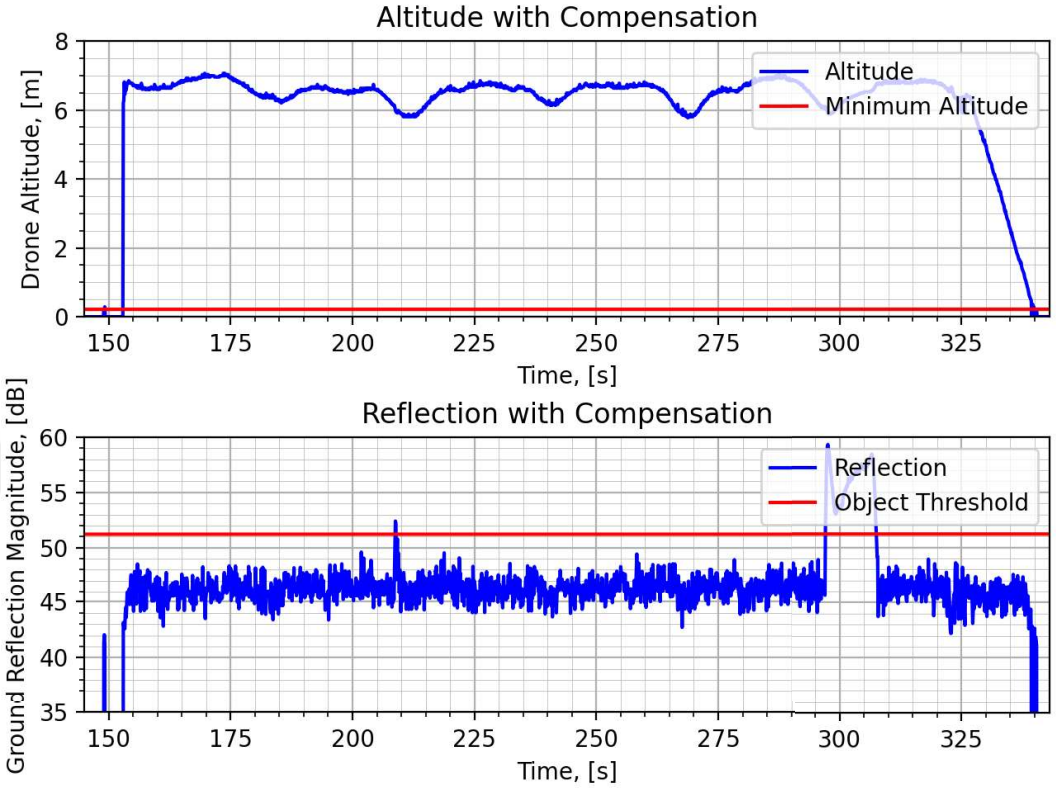

Figure 4.11. Detected altitude and reflection against time for the flight duration with range compensation.

5. CONCLUSION

A radar-equipped drone system is proposed for UAV positioning applications. The radar incorporated is IWR1843BOOST of Texas Instruments, an evaluation module of an industrial FMCW radar chip which works between 76GHz and 81GHz with 4GHz continuous transmission bandwidth. The radar module is able to transfer range profiles obtained and relative object positions and velocities detected within a frame period. An embedded computer board, Nvidia Jetson AGX Xavier Developer Kit, is used to operate as an acquisition and processing platform which is responsible from configuring and starting the radar sensor and storing received radar data, all in ROS environment, in addition to providing computational resources to other applications. A custom drone system is designed and manufactured using relatively inexpensive parts, on which the radar sensor and the processing platform are mounted.

A field experiment is done at the Uçaksavar Stadium of Boğaziçi University. Firstly, the experimental results show that proposed FMCW radar system and post-processing methods can be used to detect the altitude above ground level and the magnitude of the ground reflections. However, ground reflection values vary by the range value. To overcome this problem, a range compensation method is proposed, which resembles path loss compensation. Ground reflection values obtained from different ranges become similar with this solution. Minimum detectable altitude is also improved. The objects placed on the ground were successfully distinguished from the ground in the experiment.

The success on the field test shows that proposed radar system can be used in UAV positioning applications. The landing period in Figure 4.11 clearly shows that one such example is landing aid. The radar system can provide information that can be useful for navigation of a UAV by making use of the described postprocessing steps which can be applied near real-time onboard. This is an important advancement because of the fact that the airborne radar systems which are lately started to be used on small UAVs

mostly do not involve sufficient computational resources for onboard postprocessing and they transfer the data to a ground station for postprocessing. Radar systems were only usable on heavy airborne vehicles with similar purposes before. Apart from some recently emerging agricultural drones that use radars in simple obstacle avoidance tasks, studies in literature transfer or store data to perform postprocessing later on ground without using for navigation. Radar reflection information is also provided by the radar system, which may help collecting information about material properties. Furthermore, the onboard processing platform can provide resources for additional applications such as SAR imaging or more advanced detection algorithms.

Proposed drone system can be equipped with RTK sensor to obtain more accurate positioning information so that more comprehensive experimental flights can be realized. Accurate position information also enables advanced applications such as SAR imaging, which can be performed using a backprojection algorithm. Such an algorithm can be implemented on the processing platform of the radar system as its GPU cores allow parallel processing and speed up the generation of a final image.

Other types of sensors which are capable of detecting distance such as lidars can also be employed on the system so that the measurement results obtained with the radar can be compared to the output of these sensors. Currently, the radar is able to state an altitude value, which is measured with respect to the ground level. Using other sensors to measure the orientation and the altitude with respect to the mean sea level of the drone with a similar precision to the radar can allow applications such as terrain mapping.

The radar system can report an altitude value in ROS environment and, theoretically, a flight controller can use this information. This step is not realized in this work as it is a compelling job by itself. An open-source autopilot software is used in this work as it is. A new autopilot software that can take the altitude measurement obtained with the radar into account for navigating the drone can be developed.

Another enhancement that would enable better experiment plans is to use a more advanced drone system. Although small UAVs are becoming more available each day, their costs can still be high for research. The components used in the proposed drone system are relatively low cost. A drone system that can endure longer flight durations would allow denser C-scans, increasing the number of measurements taken over an area. Commercially available UAVs may provide this with open-source autopilots at lower costs in the future.

In summary, sensor systems and application areas of modern small UAVs are explored. Literature is reviewed to find drone applications that use radars. State of the art in drone radar systems is examined. The working principles and theoretical limitations of FMCW radars are analyzed. A broad survey is done to discover the available FMCW radar sensors which are usable on small drone platforms. An FMCW radar system is designed and an altitude and object detection algorithm is developed to be used in positioning applications. A custom drone system is designed and implemented to carry the radar system. Experimental results show that the system and the algorithm successfully obtains the altitude and detects ground reflections as well as the existence of objects.

REFERENCES

1. Chakrabarty, A., R. Morris, X. Bouyssounouse and R. Hunt, "Autonomous Indoor Object Tracking with the Parrot AR. Drone", *International Conference on Unmanned Aircraft Systems (ICUAS)*, pp. 25–30, Arlington, VA, USA, 2016.

2. González-Jorge, H., J. Martínez-Sánchez, M. Bueno and P. Arias, "Unmanned Aerial Systems for Civil Applications: A Review", *Drones*, Vol. 1, No. 1, p. 2, 2017.

3. Theodorakopoulos, P. and S. Lacroix, "A Strategy for Tracking a Ground Target with a UAV", *IEEE/RSJ International Conference on Intelligent Robots and Systems*, pp. 1254–1259, Nice, France, 2008.

4. Everaerts, J., "The Use of Unmanned Aerial Vehicles (UAVs) for Remote Sensing and Mapping", *The International Archives of the Photogrammetry, Remote Sensing and Spatial Information Sciences*, Vol. 37, No. 2008, pp. 1187–1192, 2008.

5. Ma'Sum, M. A., M. K. Arrofi, G. Jati, F. Arifin, M. N. Kurniawan, P. Mursanto and W. Jatmiko, "Simulation of Intelligent Unmanned Aerial Vehicle (UAV) for Military Surveillance", *International Conference on Advanced Computer Science and Information Systems (ICACSIS)*, pp. 161–166, Sanur Bali, Indonesia, 2013.

6. Dong, J., K. Ota and M. Dong, "UAV-based Real-Time Survivor Detection System in Post-Disaster Search and Rescue Operations", *IEEE Journal on Miniaturization for Air and Space Systems*, Vol. 2, No. 4, pp. 209–219, 2021.

7. Georgiev, G. D., G. Hristov, P. Zahariev and D. Kinaneva, "Forest Monitoring System for Early Fire Detection Based on Convolutional Neural Network and UAV imagery", *28th National Conference with International Participation (TELECOM)*, pp. 57–60, Sofia, Bulgaria, 2020.

8. Salvo, G., L. Caruso and A. Scordo, "Urban Traffic Analysis through an UAV", *Procedia-Social and Behavioral Sciences*, Vol. 111, pp. 1083–1091, 2014.

9. Stehr, N. J., "Drones: The Newest Technology for Precision Agriculture", *Natural Sciences Education*, Vol. 44, No. 1, pp. 89–91, 2015.

10. Bhardwaj, A., L. Sam, F. J. Martín-Torres and R. Kumar, "UAVs as Remote Sensing Platform in Glaciology: Present Applications and Future Prospects", *Remote Sensing of Environment*, Vol. 175, pp. 196–204, 2016.

11. Yarlequé, M., S. Alvarez and H. Martinez, "FMCW GPR Radar Mounted in a Mini-UAV for Archaeological Applications: First Analytical and Measurement Results", *International Conference on Electromagnetics in Advanced Applications (ICEAA)*, pp. 1646–1648, Verona, Italy, 2017.

12. Garcia-Fernandez, M., Y. Alvarez-Lopez and F. Las Heras, "Autonomous Airborne 3D SAR Imaging System for Subsurface Sensing: UWB-GPR On Board a UAV for Landmine and IED Detection", *Remote Sensing*, Vol. 11, No. 20, p. 2357, 2019.

13. Fernández, M. G., Y. Á. López, A. A. Arboleya, B. G. Valdés, Y. R. Vaqueiro, F. L.-H. Andrés and A. P. García, "Synthetic Aperture Radar Imaging System for Landmine Detection Using a Ground Penetrating Radar On Board a Unmanned Aerial Vehicle", *IEEE Access*, Vol. 6, pp. 45100–45112, 2018.

14. García-Fernández, M., Y. Á. López and F. L.-H. Andrés, "Airborne Multi-Channel Ground Penetrating Radar for Improvised Explosive Devices and Landmine Detection", *IEEE Access*, Vol. 8, pp. 165927–165943, 2020.

15. Colorado, J., M. Perez, I. Mondragon, D. Mendez, C. Parra, C. Devia, J. Martinez-Moritz and L. Neira, "An Integrated Aerial System for Landmine Detection: SDR-based Ground Penetrating Radar Onboard an Autonomous Drone", *Advanced Robotics*, Vol. 31, No. 15, pp. 791–808, 2017.

16. Burr, R., M. Schartel, P. Schmidt, W. Mayer, T. Walter and C. Waldschmidt, "Design and Implementation of a FMCW GPR for UAV-based Mine Detection", *IEEE MTT-S International Conference on Microwaves for Intelligent Mobility (ICMIM)*, pp. 1–4, Munich, Germany, 2018.

17. Burr, R., M. Schartel, W. Mayer, T. Walter and C. Waldschmidt, "UAV-based Polarimetric Synthetic Aperture Radar for Mine Detection", *IGARSS IEEE International Geoscience and Remote Sensing Symposium*, pp. 9208–9211, Yokohama, Japan, 2019.

18. Schreiber, E., A. Heinzel, M. Peichl, M. Engel and W. Wiesbeck, "Advanced Buried Object Detection by Multichannel, UAV/Drone Carried Synthetic Aperture Radar", *13th European Conference on Antennas and Propagation (EuCAP)*, pp. 1–5, Krakow, Poland, 2019.

19. Ham, Y., K. K. Han, J. J. Lin and M. Golparvar-Fard, "Visual Monitoring of Civil Infrastructure Systems via Camera-Equipped Unmanned Aerial Vehicles (UAVs): A Review of Related Works", *Visualization in Engineering*, Vol. 4, No. 1, pp. 1–8, 2016.

20. Kaniewski, P., C. Leśnik, W. Susek and P. Serafin, "Airborne Radar Terrain Imaging System", *16th International Radar Symposium (IRS)*, pp. 248–253, Dresden, Germany, 2015.

21. Ye, E., G. Shaker and W. Melek, "Lightweight Low-Cost UAV Radar Terrain Mapping", *13th European Conference on Antennas and Propagation (EuCAP)*, pp. 1–5, Krakow, Poland, 2019.

22. Li, C. J. and H. Ling, "High-Resolution, Downward-Looking Radar Imaging Using a Small Consumer Drone", *IEEE International Symposium on Antennas and Propagation (APSURSI)*, pp. 2037–2038, Fajardo, PR, USA, 2016.

23. Li, C. J. and H. Ling, "Synthetic Aperture Radar Imaging Using a Small Consumer Drone", *IEEE International Symposium on Antennas and Propagation & USNC/URSI National Radio Science Meeting*, pp. 685–686, Vancouver, BC, Canada, 2015.

24. Virone, G., A. M. Lingua, M. Piras, A. Cina, F. Perini, J. Monari, F. Paonessa, O. A. Peverini, G. Addamo and R. Tascone, "Antenna Pattern Verification System Based on a Micro Unmanned Aerial Vehicle (UAV)", *IEEE Antennas and Wireless Propagation Letters*, Vol. 13, pp. 169–172, 2014.

25. García-Fernández, M., Y. Á. López, A. Arboleya, B. González-Valdés, Y. Rodríguez-Vaqueiro, M. E. D. C. Gómez and F. L.-H. Andrés, "Antenna Diagnostics and Characterization Using Unmanned Aerial Vehicles", *IEEE Access*, Vol. 5, pp. 23563–23575, 2017.

26. Suherman, S., R. A. Putra and M. Pinem, "Ultrasonic Sensor Assessment for Obstacle Avoidance in Quadcopter-based Drone System", *3rd International Conference on Mechanical, Electronics, Computer, and Industrial Technology (MECnIT)*, pp. 50–53, Medan, Indonesia, 2020.

27. Peng, Z., J. M. Muñoz-Ferreras, Y. Tang, C. Liu, R. Gómez-García, L. Ran and C. Li, "A Portable FMCW Interferometry Radar with Programmable Low-IF Architecture for Localization, ISAR Imaging, and Vital Sign Tracking", *IEEE Transactions on Microwave Theory and Techniques*, Vol. 65, No. 4, pp. 1334–1344, 2016.

28. Meta, A., P. Hoogeboom and L. P. Ligthart, "Signal Processing for FMCW SAR", *IEEE Transactions on Geoscience and Remote Sensing*, Vol. 45, No. 11, pp. 3519–3532, 2007.

29. Yan, J., Z. Peng, H. Hong, X. Zhu, Q. Lu, B. Ren and C. Li, "Indoor Range-Direction-Movement SAR for Drone-based Radar Systems", *IEEE Asia Pacific Microwave Conference (APMC)*, pp. 1290–1293, Kuala Lumpar, 2017.

30. Ding, M., X. Liang, L. Tang, Z. Wen, X. Wang and Y. Wang, "Micro FMCW SAR with High Resolution for Mini UAV", *International Conference on Microwave and Millimeter Wave Technology (ICMMT)*, pp. 1–3, Chengdu, China, 2018.

31. Lort, M., A. Aguasca, C. Lopez-Martinez and T. M. Marín, "Initial Evaluation of SAR Capabilities in UAV Multicopter Platforms", *IEEE Journal of Selected Topics in Applied Earth Observations and Remote Sensing*, Vol. 11, No. 1, pp. 127–140, 2017.

32. Ding, M.-L., C.-B. Ding, L. Tang, X.-M. Wang, J.-M. Qu and R. Wu, "A W-band 3-D Integrated Mini-SAR System with High Imaging Resolution on UAV Platform", *IEEE Access*, Vol. 8, pp. 113601–113609, 2020.

33. Svedin, J., A. Bernland, A. Gustafsson, E. Claar and J. Luong, "Small UAV-based SAR System Using Low-Cost Radar, Position, and Attitude Sensors with Onboard Imaging Capability", *International Journal of Microwave and Wireless Technologies*, Vol. 13, No. 6, pp. 602–613, 2021.

34. Patole, S. M., M. Torlak, D. Wang and M. Ali, "Automotive Radars: A Review of Signal Processing Techniques", *IEEE Signal Processing Magazine*, Vol. 34, No. 2, pp. 22–35, 2017.

35. Rao, S., A. Ahmad, J. C. Roh and S. Bharadwaj, "77GHz Single Chip Radar Sensor Enables Automotive Body and Chassis Applications", Texas Instruments, Dallas, TX, 2017.

36. Wang, F.-K., T.-S. Horng, K.-C. Peng, J.-K. Jau, J.-Y. Li and C.-C. Chen, "Detection of Concealed Individuals Based on Their Vital Signs by Using a See-Through-Wall Imaging System with a Self-Injection-Locked Radar", *IEEE Transactions on Microwave Theory and Techniques*, Vol. 61, No. 1, pp. 696–704, 2012.

37. Wang, F.-K., T.-S. Horng, K.-C. Peng, J.-K. Jau, J.-Y. Li and C.-C. Chen, "See-

ing Through Walls with a Self-Injection-Locked Radar to Detect Hidden People", *IEEE/MTT-S International Microwave Symposium Digest*, pp. 1–3, Montreal, QC, Canada, 2012.

38. Gunn, G. E., C. R. Duguay, D. K. Atwood, J. King and P. Toose, "Observing Scattering Mechanisms of Bubbled Freshwater Lake Ice Using Polarimetric RADARSAT-2 (C-Band) and UW-Scat (X-and Ku-Bands)", *IEEE Transactions on Geoscience and Remote Sensing*, Vol. 56, No. 5, pp. 2887–2903, 2018.

39. Wang, H., M. Jiang and S. Zheng, "Airborne Ka FMCW MiSAR System and Real Data Processing", *17th International Radar Symposium (IRS)*, pp. 1–5, Krakow, Poland, 2016.

40. Lampersberger, T., R. Feger, A. Haderer, C. Egger, M. Friedl and A. Stelzer, "A 24-GHz Radar with 3D-Printed and Metallized Lightweight Antennas for UAV Applications", *15th European Radar Conference (EuRAD)*, pp. 393–396, Madrid, Spain, 2018.

41. "IWR1843 Single-Chip 76- to 81-GHz FMCW mmWave Sensor Datasheet (Rev. A)", Texas Instruments, Dallas, TX, 2022.

42. "AWR1843BOOST and IWR1843BOOST Single-Chip mmWave Sensing Solution User's Guide (Rev. B)", Texas Instruments, Dallas, TX, 2020.

43. Ramasubramanian, K., "Using a Complex-Baseband Architecture in FMCW Radar Systems", Texas Instruments, Dallas, TX, 2017.